Ferromagnetic versus Antiferromagnetic Exchange in Five Structurally Analogous Carboxylate-Bridged Trinuclear Ferrous Complexes

David P. Goldberg,[†] Joshua Telser,[‡] Cecilia M. Bastos,[†] and Stephen J. Lippard*,[†]

Departments of Chemistry, Massachusetts Institute of Technology, Cambridge, Massachusetts 02139, and Roosevelt University, Chicago, Illinois 60605

Received November 18, 1994[⊗]

The synthesis, structural characterization, and magnetic properties of linear, trinuclear complexes of general formula $[Fe_3(O_2CR)_6L_2]$ are reported. Addition of $Fe(OAc)_2$ to the bidentate nitrogen donor ligands bis(1-methyl-2-imidazolyl)phenylhydroxymethane (BIPhOH) and 1,1-bis(1-methyl-2-imidazolyl)-1-(3,5-di-*tert*-butyl-4-hydroxyphenyl)ethane (BIDPhEH) afforded $[Fe_3(OAc)_6(BIPhOH)_2]\cdot 2MeOH$ (**3**) and $[Fe_3(OAc)_6(BIDPhEH)_2]$ (**4**), respectively. Complex **3** crystallizes in $P\bar{1}$, with $a = 8.985(2)$ Å, $b = 9.148(1)$ Å, $c = 15.761(2)$ Å, $\alpha = 80.73(1)°$, $\beta = 81.28(1)°$, $\gamma = 101.91(1)°$, $V = 1228.0(4)$ Å^3, and $Z = 1$ ($R = 0.046$, $R_w = 0.056$), and complex **4** crystallizes in $P2_1/n$, with $a = 12.809(5)$ Å, $b = 22.214(5)$ Å, $c = 13.793(5)$ Å, $\beta = 91.19(2)°$, $V = 3924(2)$ Å^3, and $Z = 2$ ($R = 0.055$, $R_w = 0.076$). Addition of $Fe(BF_4)_2\cdot 6H_2O$ and sodium benzoate to the ligands bis[2-((*4S*)-(1-methylethyl)-1,3-oxazolinyl)]methane (^{i}PrOx) and *N,N,N′*-trimethyl-*N′*-[4,4-dimethyl-4-(3,5-di-*tert*-butyl-4-hydroxyphenyl)butyl]ethylenediamine ($PheMe_3Eda$) yielded compounds $[Fe_3(O_2CPh)_6(^iPrOx)_2]$ (**5**) and $[Fe_3(O_2CPh)_6(PheMe_3Eda)_2]$ (**6**), respectively. Compound **5** crystallizes in $P2_12_12_1$, with $a = 14.677(3)$ Å, $b = 19.289(4)$ Å, $c = 23.066(6)$ Å, $V = 6530(4)$ Å^3, and $Z = 4$ ($R = 0.059$, $R_w = 0.065$), and compound **6** in $P2_1/n$, with $a = 10.111(1)$ Å, $b = 31.389(2)$ Å, $c = 14.243(2)$ Å, $\beta = 100.76(5)°$, $V = 4441(1)$ Å^3, and $Z = 2$ ($R = 0.047$, $R_w = 0.063$). In all of these complexes, the iron atoms are linked by two bidentate and one unidentate bridging carboxylate ligands. The coordination spheres of the terminal iron atoms are completed by the bidentate nitrogen ligands and, in compounds **5** and **6**, by the second "dangling" oxygen atom of the unidentate bridging carboxylate. We investigated the magnetic properties of these four compounds, as well as those of $[Fe_3(OAc)_6(BIPhMe)_2]$ (**1**), reported previously (Rardin, R. L.; Poganiuch, P.; Bino A.; Goldberg, D. P.; Tolman, W. B.; Liu, S.; Lippard, S. J. *J. Am. Chem. Soc.* **1992,** *114,* 5240−5249). Three of the complexes (**1**, **3**, and **4**) exhibit intramolecular ferromagnetic exchange coupling, $J = -2$ to -5 cm^{-1} ($\mathcal{H} = JS_1\cdot S_2$), resulting in high-spin $S = 6$ ground states, and the remaining two complexes are antiferromagnetically coupled, with $S = 2$ ground states. The magnetic properties thus correlate with the structural differences between the two classes of compounds. Both temperature-dependent magnetic susceptibility and high-field magnetization measurements reveal this behavior. The magnetic data were fit to a theoretical model incorporating exchange coupling, single-ion zero-field splitting, and **g** tensor anisotropy. A set of consensus magnetic parameters for each compound was obtained, with weak magnetic exchange ($|J| \leq 5$ cm^{-1}) between nearest-neighbor iron atoms being a common feature for all five compounds. The X-band EPR spectra of **1**, **3**, and **4** at 4 K displayed broad, low-field ($g_{obs} \approx 18$) signals consistent with integer-spin ground states. These spectra are remarkably similar to those of the reduced, diiron(II) centers found in the non-heme iron proteins methane monooxygenase (MMOH), hemerythrin (Hr), and the R2 protein of ribonucleotide reductase. Theoretical calculations indicate that several allowed EPR transitions from the resulting manifold of ground and low-lying excited energy levels arising from the integer spin ($S = 6$) state could be responsible for the broad low-field absorption feature.

Introduction

The fully-reduced forms of the non-heme iron proteins methane monooxygenase hydroxylase (MMOH), ribonucleotide reductase R2 (R2), and hemerythrin (Hr) all contain a carboxylate-bridged diiron(II) active site in which the iron atoms are additionally coordinated to imidazole and carboxylate functionalities.[1−3] Understanding the structural and electronic properties of the diiron(II) centers in these proteins is an important part of deriving their functional mechanisms. Significant progress has been made in characterizing the magnetic behavior of all three proteins in their reduced forms. Weak ferromagnetic exchange coupling has been reported for $MMOH_{red}$ ($\mathcal{H} = JS_1\cdot S_2$), $J = -0.6$ to -1.0 cm^{-1},[4] for $R2_{red}$, $J = -0.6$ cm^{-1},[5] and for deoxyHrN_3, $J = -3.4$ cm^{-1}.[6] For both $MMOH_{red}$[7−9] and deoxyHrN_3,[6,10] a low-field integer-spin EPR signal ($g_{obs} \approx 16$) has been observed, and recently ESEEM and ENDOR spectra were obtained by utilizing this signal.[11] The

[†] Massachusetts Institute of Technology.
[‡] Roosevelt University.
[⊗] Abstract published in *Advance ACS Abstracts,* April 15, 1995.

(1) Feig, A. L.; Lippard, S. J. *Chem. Rev.* **1994,** *94,* 759−805.
(2) Que, L., Jr.; True, A. E. *Prog. Inorg. Chem.* **1990,** *38,* 97−200.
(3) Vincent, J. B.; Olivier-Lilley, G. L.; Averill, B. A. *Chem. Rev.* **1990,** *90,* 1447−1467.
(4) Pulver, S.; Froland, W. A.; Fox, B. G.; Lipscomb, J. D.; Solomon, E. I. *J. Am. Chem. Soc.* **1993,** *115,* 12409−12422.
(5) Atta, M.; Scheer, C.; Fries, P. H.; Fontecave, M.; Latour, J.-M. *Angew. Chem., Int. Ed. Engl.* **1992,** *31,* 1513−1515.
(6) Hendrich, M. P.; Pearce, L. L.; Que, L., Jr.; Chasteen, D.; Day, E. P. *J. Am. Chem. Soc.* **1991,** *113,* 3039−3044.
(7) DeWitt, J. G.; Bentsen, J. G.; Rosenzweig, A. C.; Hedman, B.; Green, J.; Pilkington, S.; Papaefthymiou, G. C.; Dalton, H.; Hodgson, K. O.; Lippard, S. J. *J. Am. Chem. Soc.* **1991,** *113,* 9219−9235.
(8) Hendrich, M. P.; Münck, E.; Fox, B. G.; Lipscomb, J. D. *J. Am. Chem. Soc.* **1990,** *112,* 5861−5865.
(9) Fox, B. G.; Surerus, K. K.; Münck, E.; Lipscomb, J. D. *J. Biol. Chem.* **1988,** *263,* 10553−10556.
(10) Reem, R. C.; Solomon, E. I. *J. Am. Chem. Soc.* **1987,** *109,* 1216−1226.

0020-1669/95/1334-3011$09.00/0

origin of the low-field EPR signal was in all cases attributed to a weakly ferromagnetically coupled diiron(II) system, a conclusion supported in the case of deoxyHrN_3 by magnetic susceptibility measurements.[6] For $R2_{red}$, a similar low-field EPR signal was described,[12] which can be altered upon addition of azide ion.[13]

A small number of carboxylate-bridged diiron(II) complexes are available as models for the protein iron cores. The compounds $[Fe_2(\mu\text{-}OH)(\mu\text{-}OAc)_2(Me_3TACN)_2](ClO_4)$[14,15] and $[Fe_2(\mu\text{-}OH_2)(\mu\text{-}OAc)_2(OAc)_2(tmen)_2]$[16] contain bridging hydroxide and water ligands, respectively, as well as two bidentate bridging carboxylates. Antiferromagnetic coupling ($J = 26$ cm^{-1}) has been observed for the former compound and very weak coupling for the latter. The alkoxo-, carboxylato-bridged complex $[Fe_2(OBz)(N\text{-Et-HPTB})](BF_4)_2$ also exhibits antiferromagnetic exchange ($J = 22$ cm^{-1}).[17] None of these compounds has been reported to have EPR signals. An analogous phenoxo-bridged complex, $[Fe_2(O_2CR)_2(BPMP)](BPh_4)$ (R = C_2H_5, Ph),[18] displays weak ferromagnetic coupling and a broad, low-field $g \approx 16$ EPR signal; similar results were recently obtained for the analogous compound $[Fe_2(O_2CPh)_2(BPCP)](BPh_4)$.[19] Other diiron(II) complexes having weak ($0 \geq J \geq -10$ cm^{-1}) ferromagnetic coupling and low-field EPR signals include the bis(phenoxo)-bridged complex $[Fe_2(H_2Hbab)_2(N\text{-MeIm})_2]$,[20] and a series of bis(μ-halo) complexes of the type $[Fe_2L_2X_2]$, where L = TLA, TMPzA, or TPA and X = Cl or F.[21] Another bis(phenoxo)-bridged complex, $[Fe_2(salmp)_2]^{2-}$,[22] was initially described as being weakly ferromagnetically coupled with $J = -2.46$ cm^{-1}. This compound was recently reinvestigated and found to have a significantly more negative J value of -13.7 cm^{-1}, obtained by fitting magnetization and Mössbauer data to a model incorporating zero-field splitting parameters.[23] The complex $[Fe_2(O_2CH)_4(BIPhMe)_2]$,[24] which contains a monodentate-bridging and two bidentate-bridging formate ligands, exhibits little or no magnetic exchange coupling. A fit of the magnetic susceptibility data gave $J = 0.32$ cm^{-1}, without inclusion of zero-field splitting parameters. This compound also displayed a low-field EPR signal.[25] The magnitude of J for these diiron(II) complexes is quite small compared to the values of related (μ-oxo)bis(μ-carboxylato)diiron(III) complexes, which are in the 160−260 cm^{-1} range.[2,26] Significant zero-field splitting (zfs) for high-spin ferrous ion makes it more difficult to fit the magnetic data for the Fe(II) complexes, especially when the zfs effects are of the same magnitude as the exchange coupling interaction.[10]

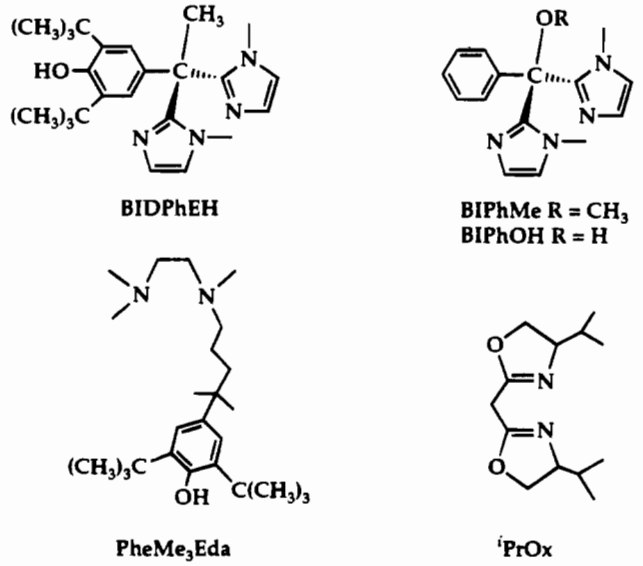

Figure 1. Bidentate nitrogen donor ligands used in this study.

In the course of our continuing studies of synthetic models for the various forms of the carboxylate-bridged diiron centers in the reaction cycles of MMOH, Hr, and R2, we have prepared a series of similar, but structurally and magnetochemically distinguishable, trinuclear ferrous complexes. Compounds of the general formula $[Fe_3(O_2CR)_6L_2]$, where L is one of the bidentate nitrogen donor ligands depicted in Figure 1, have been synthesized and characterized. Although the desired dinuclear structural type could not be obtained with simple carboxylate bridging ligands, the resulting triiron(II) complexes are of considerable interest in their own right and relevant to the natural systems. The linear arrangement of metal atoms allows each "half" of the complex to be viewed as a dinuclear unit, and it is useful to compare the nature of the magnetic coupling between adjacent iron atoms in these trinuclear systems with that in the analogous dinuclear protein cores.

In the present article we report the synthesis, magnetic susceptibility, high-field magnetization and EPR properties, and electronic structures of these complexes. We also describe a procedure for fitting the magnetic susceptibility and high-field magnetization data to a theoretical model which incorporates zero-field splitting effects and single-ion **g** anisotropy. This model is more general than the conventional analytical method based on the Kambé coupling scheme and Van Vleck equations[27,28] and should be of value in treating low-nuclearity polyiron(II) systems. One of these complexes, $[Fe_3(OAc)_6(BIPhMe)_2]$ (**1**), was previously reported to be ferromagnetically coupled.[29] The magnetic properties of this complex have been

(11) Hoffman, B. M.; Sturgeon, B. E.; Doan, P. E.; DeRose, V. J.; Liu, K. E.; Lippard, S. J. *J. Am. Chem. Soc.* **1994**, *116*, 6023−6024.
(12) Lynch, J. B.; Juarez-Garcia, C.; Münck, E.; Que, L., Jr. *J. Biol. Chem.* **1989**, *264*, 8091−8096.
(13) Elgren, T. E.; Hendrich, M. P.; Que, L., Jr. *J. Am. Chem. Soc.* **1993**, *115*, 9291−9292.
(14) Hartman, J. R.; Rardin, R. L.; Chaudhuri, P.; Pohl, K.; Wieghardt, K.; Nuber, B.; Weiss, J.; Papaefthymiou, G. C.; Frankel, R. B.; Lippard, S. J. *J. Am. Chem. Soc.* **1987**, *109*, 7387−7396.
(15) Abbreviations used: Me_3TACN, 1,4,7-trimethyl-1,4,7-triazacyclononane; tmen, *N,N,N′,N′*-tetramethyl-1,2-diaminoethane; BPMP, the anion of 2,6-bis[[bis(2-pyridylmethyl)amino]methyl]-4-methylphenol; BPCP, the anion of 2,6-bis[[bis(2-pyridylmethyl)amino]methyl]-4-chlorophenol; HPTBP, *N,N,N′,N′*-tetrakis(2-benzimidazolylmethyl)-2-hydroxy-1,3-diaminopropane; H_4Hbab, 1,2-bis(2-hydroxybenzamido)benzene; SALMP, bis(salicylideneamino)-2-methylphenolate(3−); TLA, tris(6-methyl-2-pyridylmethyl)amine; TMPzA, tris[(3,5-dimethyl-1-pyrazolyl)methyl]amine; TPA, tris(2-pyridylmethyl)amine.
(16) Hagen, K. S.; Lachicotte, R. *J. Am. Chem. Soc.* **1992**, *114*, 8741−8742.
(17) Ménage, S.; Brennan, B. A.; Juarez-Garcia, C.; Münck, E.; Que, L., Jr. *J. Am. Chem. Soc.* **1990**, *112*, 6423−6425.
(18) Borovik, A. S.; Hendrich, M. P.; Holman, T. R.; Münck, E.; Papaefthymiou, V.; Que, L., Jr. *J. Am. Chem. Soc.* **1990**, *112*, 6031−6038.
(19) Jang, H. G.; Hendrich, M. P.; Que, L., Jr. *Inorg. Chem.* **1993**, *32*, 911−918.
(20) Stassinopoulos, A.; Schulte, G.; Papaefthymiou, G. C.; Caradonna, J. P. *J. Am. Chem. Soc.* **1991**, *113*, 8686−8697.
(21) Zang, Y.; Jang, H. G.; Chiou, Y.-M.; Hendrich, M. P.; Que, L., Jr. *Inorg. Chim. Acta* **1993**, *213*, 41−48.
(22) Snyder, B. S.; Patterson, G. S.; Abrahamson, A. J.; Holm, R. H. *J. Am. Chem. Soc.* **1989**, *111*, 5214−5223.
(23) Hendrich, M. P.; Day, E. P.; Wang, C.-P.; Snyder, B. S.; Holm, R. H.; Münck, E. *Inorg. Chem.* **1994**, *33*, 2848−2856.
(24) Tolman, W. B.; Liu, S.; Bentsen, J. G.; Lippard, S. J. *J. Am. Chem. Soc.* **1991**, *113*, 152−164.
(25) This low-field EPR signal is currently being further investigated: Hendrich, M. P.; Herold, S.; Goldberg, D. P; Lippard, S. J. Unpublished results.
(26) Kurtz, D. M., Jr. *Chem. Rev.* **1990**, *90*, 585−606.
(27) Kambé, K. *J. Phys. Soc. Jpn.* **1950**, *5*, 48−51.
(28) Sinn, E. *Coord. Chem. Rev.* **1970**, *5*, 313−347.

reinvestigated, and the initial qualitative description has been confirmed. We have now determined, however, that the magnetic moment obtained from the original measurement was artificially high, owing to partial mechanical torquing of the crystallites in the applied field.

Experimental Section

General Methods. Unless otherwise noted, materials were obtained from commercial sources and used as received. All manipulations and reactions were carried out under an inert atmosphere in a Vacuum Atmospheres drybox or by using standard Schlenk techniques. Solvents THF, diethyl ether, pentane, and toluene were distilled from Na/benzophenone ketyl under nitrogen; CH_2Cl_2 and methanol were distilled from CaH_2 and magnesium methoxide, respectively, under nitrogen. The ligands (Figure 1) bis[2-((*4S*)-(1-methylethyl)-1,3-oxazolinyl)]-methane (^{i}PrOx),[30] bis(1-methyl-2-imidazolyl)phenylhydroxymethane (BIPhOH),[24] bis(1-methyl-2-imidazolyl)phenylmethoxymethane (BIPhMe),[24] and 1,1-bis(1-methyl-2-imidazolyl)-1-(3,5-di-*tert*-butyl-4-hydroxyphenyl)ethane (BIDPhEH)[31] were prepared according to literature procedures. ^{1}H and ^{13}C NMR spectra were recorded on a Bruker AC 250 spectrometer. Proton resonances, reported in units of ppm downfield from tetramethylsilane (TMS), were referenced to residual solvent protons. Electron-impact (EI) mass spectra were obtained on a Finnigan MAT 8200 mass spectrometer.

3,5-Di-*tert*-butyl-4-hydroxyphenyl 3-Chloropropyl Ketone (2a). A portion of 4-chlorobutyryl chloride (39.0 mL, 0.348 mol) was added to a previously cooled (−78 °C) solution of 2,6-di-*tert*-butylphenol (71.53 g, 0.347 mol) in CH_2Cl_2 (400 mL). A 45.0 g (0.338 mol) quantity of $AlCl_3$ was added slowly to this solution. The mixture was stirred at −78 °C for 1 h and then warmed slowly to room temperature. The mixture was quenched by slow addition to an ice-cold solution of HCl (400 g of ice and 10 mL of concentrated HCl), and the product was extracted with ethyl acetate (5 × 200 mL). The organic layer was dried over $MgSO_4$ and filtered, and the solvent was removed in vacuo. The crude product was purified by chromatography on a silica column (5% [v/v] ethyl acetate in CH_2Cl_2), affording 65.5 g (61%) of a white solid: ^{1}H NMR ($CDCl_3$) δ 1.48 (s, 18H, $C(CH_3)_3$), 2.23 (quintet, 2H, J = 6.4 Hz, CH_2), 3.14 (t, 2H, J = 6.4 Hz, $C(O)CH_2$), 3.69 (t, 2H, J = 6.4 Hz, CH_2Cl), 5.75 (s, 1H, OH), 7.88 (s, 2H, C_6H_2); ^{13}C NMR ($CDCl_3$) δ 27.24, 30.02, 34.23, 34.58, 44.56, 125.60, 128.58, 135.84, 158.39, 198.12; mass spectrum (EI) *m/e* 310 (M^+).

2,6-Di-*tert*-butyl-4-(1,1-dimethyl-4-chlorobutyl)phenol (2b). A 3 mL aliquot of a 1 M solution of $TiCl_4$ in CH_2Cl_2 (3.0 mmol) was dissolved in CH_2Cl_2 (15 mL), and the solution was cooled to −40 °C. To this solution was slowly added a 2 M solution of dimethylzinc in toluene (1.5 mL, 3.0 mmol). The mixture was stirred at −40 °C for 45 min. A solution of **2a** (0.4776 g, 1.54 mmol) in CH_2Cl_2 (10 mL) was added slowly to the reaction mixture, which turned from colorless to orange. The resulting solution was stirred at −40 °C for 2 h and warmed to room temperature over a period of 3 h. The reaction mixture was poured into an ice-cold solution of 1 N HCl (20 mL) over approximately 100 mL of ice and then extracted with CH_2Cl_2 (3 × 40 mL). The organic layer was dried over $MgSO_4$ and filtered, and the solvent was removed in vacuo. The product was purified by chromatography on a silica column (1% [v/v] ethyl acetate in hexane), affording 0.372 g (74%) of a white solid: ^{1}H NMR ($CDCl_3$) δ 1.30 (s, 6H, $C(CH_3)_2$), 1.45 (s, 18H, $C(CH_3)_3$), 1.50−1.72 (m, 4H, $(CH_2)_2$), 3.43 (t, 2H, CH_2Cl), 5.05 (s, 1H, OH), 7.12 (s, 2H, C_6H_2); ^{13}C NMR ($CDCl_3$) δ 28.71, 29.23, 30.50, 34.58, 37.26, 41.88, 45.81, 122.22, 135.18, 139.14, 151.44; mass spectrum (EI) *m/e* 324 (M^+).

***N,N,N′*-Trimethyl-*N′*-[4,4-dimethyl-4-(3,5-di-*tert*-butyl-4-hydroxyphenyl)butyl]ethylenediamine (PheMe$_3$Eda) (2c).** An amount of **2b** (8.75 g, 26.9 mmol) was added to *N,N,N′*-trimethylethylenediamine (12.70 g, 124 mmol), and the mixture was refluxed for 4 h. The unreacted *N,N,N′*-trimethylethylenediamine was removed by vacuum distillation. The resulting mixture was partitioned between methylene chloride and water (100 mL/50 mL) and extracted with CH_2Cl_2 (3 × 50 mL). The organic layer was washed with brine (30 mL), dried over $MgSO_4$, and filtered, and the solvent was removed in vacuo. The product was purified by vacuum distillation, affording 8.08 g (77%) of a colorless oil: ^{1}H NMR ($CDCl_3$) δ 1.28 (s, 6H, $(CH_3)_2$), 1.44 (s, 18H, $(CH_3)_3$), 1.5 (m, 4H, $(CH_2)_2$), 2.21 (s, 3H, N′−CH_3), 2.26 (s, 6H, N−$(CH_3)_2$), 2.3 (t, 2H, N′−CH_2), 2.46 (m, 4H, N-$(CH_2)_2$-N′), 5.05 (s, 1H, OH), 7.12 (s, 2H, C_6H_3); ^{13}C ($CDCl_3$) δ 22.20, 28.92, 30.35, 34.39, 37.26, 42.15, 45.45, 50.14, 54.94, 56.70, 58.68, 122.06, 134.91, 139.53, 151.17; mass spectrum (EI) *m/e* 390 (M^+).

[Fe$_3$(OAc)$_6$(BIPhOH)$_2$]·2MeOH (3). To a suspension of $Fe(OAc)_2$ (0.22 g, 1.3 mmol) in MeOH (5 mL) was added BIPhOH (0.23 g, 0.86 mmol) to give a light green slurry. This slurry was stirred for 12 h and filtered. Vapor diffusion of THF into the filtrate gave 0.20 g (41%) of **3** as a colorless crystalline solid, which was washed with THF and dried under vacuum for 15 min. Anal. Calcd for $Fe_3C_{44}H_{58}O_{16}N_8$ (M_r 1122.53): C, 47.08; H, 5.21; N, 9.98. Found: C, 46.99; H, 5.16; N, 9.91.

[Fe$_3$(OAc)$_6$(BIDPhEH)$_2$] (4). To a suspension of $Fe(OAc)_2$ (0.23 g, 1.34 mmol) in MeOH (6 mL) was added BIDPhEH (0.34 g, 0.86 mmol) in MeOH (4 mL) to give a light green slurry. This slurry was stirred for 12 h to ensure dissolution of the $Fe(OAc)_2$, at which point the solvent was removed in vacuo. The resulting white solid was redissolved in CH_3CN (20 mL) with heating to boil, and the solution was filtered while hot. Vapor diffusion of diethyl ether into CH_3CN gave **4** as a colorless crystalline solid (0.45 g, 79% yield). The supernatant was decanted, and the crystals were washed with diethyl ether and dried in vacuo for 12 h. Anal. Calcd for $C_{60}H_{86}N_8O_{14}Fe_3$ (M_r 1310.93): C, 54.97; H, 6.61; N, 8.55. Found: C, 54.89; H, 6.59; N, 8.36.

[Fe$_3$(O$_2$CPh)$_6$(^{i}PrOx)$_2$] (5). A mixture of $[Fe(H_2O)_6](BF_4)_2$ (1.216 g, 3.61 mmol), NaO_2CPh (1.701 g, 11.89 mmol), and ^{i}PrOx (0.911 g, 3.82 mmol) was dissolved in methanol (50 mL). The resulting light yellow solution was stirred for 15 min, and the solvent was removed in vacuo. The product was dissolved in toluene (100 mL), and this solution was filtered through a Celite plug. The volume of this solution was reduced, and vapor diffusion of pentane into the residual gave 0.509 g (31%) of **5** as light yellow crystals. Anal. Calcd for $Fe_3C_{68}H_{74}N_4O_{16}$ (M_r 1370.90): C, 59.58; H, 5.44; N, 4.09. Found: C, 59.42; H, 5.53; N, 4.04.

[Fe$_3$(O$_2$CPh)$_6$(PheMe$_3$Eda)$_2$] (6). A solution of $[Fe(H_2O)_6](BF_4)_2$ (0.488 g, 1.45 mmol) in MeOH (5 mL) was added to a mixture of PheMe$_3$Eda (0.571 g, 1.46 mmol) and NaO_2CPh (1.251 g, 8.68 mmol) in MeOH (20 mL). A light yellow solution and a white gel were obtained. The mixture was stirred at room temperature for 0.5 h and filtered over Celite, and the solvent was removed in vacuo. The product was extracted with benzene, the extract was filtered over Celite, and the solvent was removed in vacuo. Vapor diffusion of pentane into a CH_2Cl_2 solution of the compound afforded 0.277 g (28%) of **6** as light yellow crystals. Anal. Calcd for $Fe_3C_{92}H_{122}N_4O_{14}$ (M_r 1675.54): C, 65.95; H, 7.34; N, 3.34. Found: C, 65.27; H, 7.49; N, 3.33.

Crystallography. General Procedures. X-ray diffraction studies were performed with an Enraf-Nonius CAD-4F κ geometry diffractometer and graphite-monochromatized Mo Kā radiation (λ = 0.710 69 Å). The crystal temperature (see Table 1) was maintained by the use of an Enraf-Nonius FR558-S liquid nitrogen cryostat. The crystal specimen was transferred to a mounting stage on which it was bathed in a stream of cold nitrogen gas and mounted on the end of a quartz fiber with silicone grease. All calculations were performed with a VAXstation 4000-90 computer and the teXsan software package.[32] The Laue symmetry was determined by the unit cell parameters and confirmed by the examination of axial photographs. Two computer programs, TRANS and TRACER,[33] were employed to provide further confirmation of the choice of crystal system. The crystals were determined to be of sufficient quality for data collection as judged by

(29) Rardin, R. L.; Poganiuch, P.; Bino, A.; Goldberg, D. P.; Tolman, W. B.; Liu, S.; Lippard, S. J. *J. Am. Chem. Soc.* **1992**, *114*, 5240−5249.
(30) Lowenthal, R. E.; Abiko, A.; Masamune, S. *Tetrahedron Lett.* **1990**, *31*, 6005−6008.
(31) Goldberg, D. P.; Watton, S. P.; Masschelein, A.; Wimmer, L.; Lippard, S. J. *J. Am. Chem. Soc.* **1993**, *115*, 5346−5347.
(32) *Single Crystal Structure Analysis Software*, Version 1.6; Molecular Structure Corp.: The Woodlands, TX, 1993.
(33) Lawton, S. L. *TRACER II: A Fortran Transformation-Cell Reduction Program*; Mobil Oil Corp.: Paulsboro, NJ, 1967.

Table 1. Crystallographic Data for Complexes **3**–**6**

	3	**4**	**5**	**6**
chem formula	$Fe_3C_{44}H_{58}N_8O_{16}$	$Fe_3C_{68}H_{98}N_{12}O_{14}$	$Fe_3C_{68}H_{74}N_4O_{16}$	$Fe_3C_{92}H_{122}N_4O_{14}$
fw	1122.53	1475.14	1370.89	1675.54
space group	$P\bar{1}$	$P2_1/n$	$P2_12_12_1$	$P2_1/n$
a (Å)	8.985(2)	12.809(5)	14.677(3)	10.111(1)
b (Å)	9.148(1)	22.214(5)	19.289(4)	31.389(2)
c (Å)	15.761(2)	13.793(5)	23.066(6)	14.243(2)
α (deg)	80.73(1)			
β (deg)	81.28(1)	91.19(2)		100.76(5)
γ (deg)	101.91(1)			
V (Å^3)	1228.0(4)	3924(2)	6530(4)	4441(1)
Z	1	2	4	2
ϱ_{calcd} (g cm^{-3})	1.518	1.248	1.394	1.253
μ (cm^{-1})	9.51	6.10	7.25	5.46
$R(F_o)^a$	0.046	0.055	0.059	0.047
$R_w(F_o)^b$	0.056	0.076	0.065	0.063
λ (Å)	0.710 69	0.710 69	0.710 69	0.710 69
T (°C)	−78	−81	−80	−72

^{a} $R = \Sigma||F_o| - |F_c||/\Sigma|F_o|$ ^{b} $R_w = [(\Sigma w(|F_o| - |F_c|/\Sigma w|F_o|^2]^{1/2}$; $w = 1/\sigma^2(F_o)$.

the examination of rotational and axial photographs, the unit cell parameter errors, and the measurement of selected low-angle peak widths at half-height $\Delta\bar{w}_{1/2}$ by open-counter ω scans.

Intensity data were collected with the ω-2θ scan technique, except those for **6**, for which ω scans were used. The intensities of three standard reflections were measured after every 3600 s of exposure time. The data were corrected for Lorentz and polarization effects. The data for all complexes, with the exception of **4**, were corrected for absorption following the measurement of ψ scans.[34] The direct methods program SHELX-86[35] was used for the initial structure solutions, and final models were obtained by least-squares refinement in combination with difference Fourier syntheses. Hydrogen atoms were placed at calculated positions (C−H = 0.95 Å), and their B values were fixed at 1.2 times the B_{eq} of the atom to which they were bound, unless otherwise indicated. They were included, but not refined, in the final least-squares cycles. Scattering factors for the non-hydrogen[36] and hydrogen atoms[37] and anomalous dispersion terms[38,39] were taken from the usual sources.

An abbreviated summary of crystallographic data for **3**–**6** can be found in Table 1, and a complete listing is given in supplementary Table S1. Atomic coordinates and B_{eq} for **3**–**6** excluding those of lattice solvent and hydrogen atoms are given in Tables 2–5. Selected bond distances and angles for compounds **3**–**6** are given in Tables 6–9. Complete listings of intramolecular bond distances and angles, atomic coordinates and B_{eq}, and anisotropic thermal parameters are provided in the supplementary material, together with ORTEP diagrams of **3** and **6**.

$[Fe_3(OAc)_6(BIPhOH)_2]$·2MeOH (3). A colorless, irregular block-shaped crystal (0.30 × 0.20 × 0.10 mm), grown from MeOH/THF, was selected. The unit cell dimensions were obtained from a least-squares fit of 25 reflections in the range $10 < \theta < 15°$, and the Laue symmetry was determined to be $\bar{1}$. No decay correction was necessary during data collection since there was no significant fluctuation in the intensities of the three standard reflections. All non-hydrogen atoms were refined by using anisotropic thermal parameters. The largest positive peak in the final difference Fourier map had an electron density of 0.57 e/Å^3 and was located in the region near O(7).

$[Fe_3(OAc)_6(BIDPhEH)_2]$ (4). A colorless block-shaped crystal (0.30 × 0.35 × 0.30 mm), grown from CH_3CN/Et_2O, was selected. The unit cell dimensions were obtained from a least-squares fit of 22 reflections in the range $9 < \theta < 17°$, and the Laue symmetry was determined to be 2/*m*. No absorption correction was applied because of the minimal anisotropy in transmission factors as estimated for an average transmission curve calculated from ψ scans. No decay correction was necessary since there was no significant fluctuation in the intensities of the three standard reflections. All non-hydrogen atoms were refined by using anisotropic thermal parameters except for those of lattice solvent.

One acetonitrile molecule in the asymmetric unit was refined with isotropic thermal parameters at full occupancy. The other acetonitrile molecule was disordered over two positions with one shared carbon

Table 2. Positional Parameters and B(eq) Values for $[Fe_3(OAc)_6(BIPhOH)_2]$·2MeOH (**3**)^a

atom	x	y	z	B(eq)^b
Fe(1)	1.13464(8)	0.14942(7)	1.16609(4)	1.56(3)
Fe(2)	1.000	0	1.000	1.46(4)
O(1)	1.0304(4)	−0.0540(3)	1.1364(2)	1.9(2)
O(2)	0.9981(4)	−0.1709(4)	1.2737(2)	2.5(2)
O(3)	0.8710(4)	0.1561(4)	1.0334(2)	2.1(2)
O(4)	0.9494(4)	0.2460(4)	1.1486(2)	2.6(2)
O(5)	1.2198(4)	0.1674(4)	0.9636(2)	2.3(2)
O(6)	1.2800(4)	0.3020(4)	1.0652(2)	2.4(2)
O(7)	1.3493(4)	−0.0188(4)	1.4127(2)	2.0(2)
N(1)	1.1284(5)	0.1980(4)	1.2923(2)	1.7(2)
N(2)	1.1373(5)	0.1801(4)	1.4325(2)	1.9(2)
N(3)	1.3276(4)	0.0565(4)	1.1921(2)	1.7(2)
N(4)	1.5349(4)	0.0079(4)	1.2393(2)	1.8(2)
C(1)	1.0122(5)	−0.1757(5)	1.1950(3)	1.9(2)
C(2)	1.0112(7)	−0.3220(6)	1.1637(3)	3.0(3)
C(3)	0.8741(6)	0.2425(5)	1.0874(3)	2.0(2)
C(4)	0.7711(7)	0.3520(6)	1.0773(4)	2.9(3)
C(5)	1.3052(5)	0.2708(5)	0.9900(3)	1.8(2)
C(6)	1.4538(6)	0.3601(5)	0.9289(3)	2.2(2)
C(7)	1.3580(5)	0.1066(5)	1.3442(3)	1.4(2)
C(8)	1.4826(5)	0.2440(5)	1.3526(3)	1.6(2)
C(9)	1.5171(6)	0.3768(6)	1.2893(30)	2.0(2)
C(10)	1.6271(7)	0.5037(6)	1.2947(4)	2.8(3)
C(11)	1.7029(6)	0.4994(6)	1.3658(4)	2.6(3)
C(12)	1.6684(6)	0.3685(6)	1.4293(3)	2.5(3)
C(13)	1.5586(6)	0.2408(6)	1.4227(3)	2.1(2)
C(14)	1.2048(5)	0.1570(5)	1.3543(3)	1.6(2)
C(15)	1.0082(5)	0.2506(6)	1.3334(3)	2.0(2)
C(16)	1.0135(6)	0.2395(6)	1.4187(3)	2.3(2)
C(17)	1.1852(6)	0.1601(6)	1.5174(3)	2.7(3)
C(18)	1.4026(5)	0.0593(5)	1.2574(3)	1.5(2)
C(19)	1.4118(6)	0.0004(5)	1.1297(3)	2.0(2)
C(20)	1.5389(6)	−0.0300(5)	1.1581(3)	2.2(2)
C(21)	1.6491(6)	−0.0144(6)	1.2939(4)	2.8(3)

^{a} For atom-labeling scheme, see Figure S7. Estimated standard deviations in the least significant figure are given in parentheses. ^{b} B(eq) $= {}^8/_3\pi^2(U_{11}(aa^*)^2 + U_{22}(bb^*)^2 + U_{33}(cc^*)^2 + 2U_{12}aa^*bb^* \cos\gamma + 2U_{13}aa^*cc^* \cos\beta + 2U_{23}bb^*cc^* \cos\alpha)$.

(34) North, A. C. T.; Phillips, D. C.; Mathews, F. S. *Acta Crystallogr.* **1968**, *A24*, 351–359.
(35) Sheldrick, G. M. SHELX86. Program for crystal structure determination. University of Göttingen, Göttingen, Germany, 1986.
(36) Cromer, D. T.; Waber, J. T. In *International Tables for X-ray Crystallography*; Kynoch Press: Birmingham, U.K., 1974; Vol. 4; pp 71–98.
(37) Stewart, R. F.; Davidson, E. R.; Simpson, W. T. *J. Chem. Phys.* **1965**, *42*, 3175–3187.
(38) Ibers, J. A.; Hamilton, W. C. *Acta Crystallogr.* **1964**, *17*, 781–782.
(39) Creagh, D. C.; McAuley, W. J. In *International Tables for X-ray Crystallography*; Kluwer Academic Publishers: Dordrecht, The Netherlands, 1992; Vol. C., pp 219–222.

Table 3. Positional Parameters and B(eq) Values for $[Fe_3(OAc)_6(BIDPhEH)_2]\cdot 4CH_3CN$[a]

atom	x	y	z	B(eq)[b]
Fe(1)	0.03270(5)	0.96255(3)	0.22878(4)	2.51(3)
Fe(2)	0	1.0000	0	2.32(4)
O(1)	−0.2178(3)	0.7294(1)	0.6702(2)	3.1(1)
O(2)	0.0978(2)	0.9459(1)	0.0973(2)	2.4(1)
O(3)	0.2120(3)	0.8838(2)	0.1656(2)	3.5(2)
O(4)	−0.1394(3)	0.9832(2)	0.0860(2)	3.5(2)
O(5)	−0.1168(3)	0.9926(2)	0.2447(2)	3.7(2)
O(6)	0.0864(3)	1.0530(1)	0.2254(2)	3.7(2)
O(7)	0.0396(3)	1.0757(1)	0.0742(2)	3.2(1)
N(1)	0.0832(3)	0.9496(2)	0.3708(2)	2.3(1)
N(2)	0.1052(3)	0.9190(2)	0.5212(2)	2.5(2)
N(3)	−0.0188(3)	0.8716(2)	0.2355(3)	2.7(2)
N(4)	−0.0405(3)	0.7759(2)	0.2698(3)	2.7(2)
C(1)	0.0552(3)	0.8365(2)	0.4001(3)	2.2(2)
C(2)	0.1653(3)	0.8071(2)	0.3902(3)	2.9(2)
C(3)	−0.0131(3)	0.8067(2)	0.4759(3)	2.2(2)
C(4)	0.0197(3)	0.7600(2)	0.5341(3)	2.5(2)
C(5)	−0.0447(4)	0.7333(2)	0.6029(3)	2.6(2)
C(6)	−0.1483(3)	0.7539(2)	0.6063(3)	2.4(2)
C(7)	−0.1853(3)	0.8022(2)	0.5486(3)	2.2(2)
C(8)	−0.1152(3)	0.8278(2)	0.4850(3)	2.2(2)
C(9)	0.0031(4)	0.6829(2)	0.6688(4)	3.3(2)
C(10)	0.1213(5)	0.6853(3)	0.6725(6)	7.5(4)
C(11)	−0.0296(5)	0.6221(2)	0.6287(4)	4.6(3)
C(12)	−0.0327(7)	0.6871(3)	0.7732(4)	7.9(4)
C(13)	−0.2972(4)	0.8259(2)	0.5531(3)	2.9(2)
C(14)	−0.3759(4)	0.7760(3)	0.5255(4)	4.2(3)
C(15)	−0.3199(4)	0.8494(2)	0.6556(4)	3.9(2)
C(16)	−0.3165(4)	0.8782(2)	0.4828(4)	3.4(2)
C(17)	0.0767(3)	0.9017(2)	0.4295(3)	2.1(2)
C(18)	0.1156(4)	0.9975(2)	0.4276(3)	2.6(2)
C(19)	0.1291(4)	0.9792(2)	0.5196(3)	2.8(2)
C(20)	0.1119(5)	0.8844(2)	0.6119(3)	3.8(2)
C(21)	−0.0014(3)	0.8298(2)	0.3029(3)	2.3(2)
C(22)	−0.0703(4)	0.8443(2)	0.1588(3)	3.2(2)
C(23)	−0.0838(4)	0.7858(2)	0.1795(3)	3.2(2)
C(24)	−0.0448(5)	0.7168(2)	0.3170(4)	4.0(3)
C(25)	0.1677(4)	0.9042(2)	0.0924(3)	2.6(2)
C(26)	0.1945(5)	0.8821(2)	−0.0071(4)	4.2(3)
C(27)	−0.1739(4)	0.9898(2)	0.1694(4)	3.0(2)
C(28)	−0.2892(5)	0.9957(3)	0.1831(5)	5.8(4)
C(29)	0.0698(4)	1.0891(2)	0.1576(3)	3.0(2)
C(30)	0.0835(6)	1.1553(2)	0.1770(4)	6.0(3)

[a] For atom-labeling scheme, see Figure 3. Estimated standard deviations in the least significant figure are given in parentheses. [b] B(eq) $= {}^8/_3\pi^2(U_{11}(aa^*)^2 + U_{22}(bb^*)^2 + U_{33}(cc^*)^2 + 2U_{12}aa^*bb^* \cos\gamma + 2U_{13}aa^*cc^* \cos\beta + 2U_{23}bb^*cc^* \cos\alpha)$.

atom, C(33). This carbon atom was refined with isotropic thermal parameters at full occupancy, while the remaining electron density was modeled by C(34), C(35), N(6), and N(7), each with isotropic thermal parameters at half-occupancy. The largest positive peak in the final difference Fourier map had an electron density of 0.83 e/Å^3 and was located in the region near N(5).

$[Fe_3(O_2CPh)_6(^iPrOx)_2]$ (5). A light yellow crystal (0.33 × 0.48 × 0.45 mm) grown from pentane/CH_2Cl_2 was selected. The unit cell dimensions were obtained from a least-squares fit of 23 reflections in the range $10 < \theta < 14°$, and the Laue symmetry was revealed to be *mmm*. No decay correction was necessary since there was no significant fluctuation in the intensities of the three standard reflections. The Fe, O, and N atoms were refined with anisotropic thermal parameters, and the C atoms were refined with isotropic thermal parameters. The largest positive peak in the final difference Fourier map had an electron density of 0.54 e/Å^3 and was located in the region near C(44).

$[Fe_3(O_2CPh)_6(PheMe_3Eda)_2]$ (6). A light yellow crystal grown from pentane/CH_2Cl_2 was selected. The unit cell dimensions were obtained from a least-squares fit of 25 reflections in the range $7 < \theta < 19°$, and the Laue symmetry was 2/*m*. A decay correction was applied to account for a 2.5% loss in intensity over the 4 days of data collection. All non-hydrogen atoms were refined by using anisotropic thermal parameters. The largest positive peak in the final difference Fourier map had an electron density of 0.55 e/Å^3 and was located in the region near O(1).

Magnetic Susceptibility Studies. Solid state magnetic susceptibility measurements on 30−60 mg samples of **1** and **3**−**6** were made by using a Quantum Design MPMS SQUID magnetometer equipped with a 5.5 T magnet and operating in the range 2.5−300 K. Samples were loaded in a drybox and sealed in nitrogen-filled vials for transport to the magnetometer. Care was taken to minimize exposure of the samples to air by transferring them to the sample transport chamber of the SQUID as quickly as possible once the vial seals were broken. On several occasions, samples were immediately frozen in liquid nitrogen after removal from the magnetometer and returned to the drybox, whereupon examination of the powders revealed no observable color change, as would be expected if oxidation had taken place. The susceptibilities of the sample holder were measured at the same fields and temperatures for accurate corrections of its contribution to the total measured susceptibility. Diamagnetic corrections of -5.57×10^{-4}, -3.63×10^{-4}, -5.76×10^{-4}, -6.04×10^{-4}, and -9.62×10^{-4} cm^3/mol for **1** and **3**−**6**, respectively, were estimated from Pascal's constants[40] and subtracted from the experimental susceptibilities.

Magnetization Studies. Solid state magnetization measurements on 15−40 mg samples of **1** and **3**−**6** were made with a vibrating-sample (Foner) magnetometer at the Francis Bitter National Magnet Laboratory. Electronics were modified for use in Bitter magnets. Samples were loaded in a drybox and sealed in nitrogen-filled vials for transport to the magnetometer. Sample holders were made from Teflon or Kel-F and fitted with plungers that allowed for compression of the powders by hand to prevent mechanical torquing in the applied field. Data were collected at 2 K between 0 and 200 kOe for all samples.

EPR Studies. Spectra were recorded with a Bruker ESP-300 spectrometer equipped with an Oxford Instruments liquid-helium continuous-flow cryostat. In order to minimize partial torquing of the crystallites in the applied magnetic field during the EPR experiment, powder samples of **1**, **3**, and **4** were pressed in parafilm in a drybox, and the parafilm pellet was then loaded into a 4 mm o.d. quartz EPR tube. Samples were immediately frozen in liquid nitrogen after removal from the drybox. Centering of the solid samples in the microwave cavity was carefully done manually to maximize the signal-to-noise ratio. Diphenylpicrylhydrazyl (DDPH) or an aqueous $CuSO_4$ solution was used as a standard for calibrating the magnetic field.

Magnetic Theory and Fitting. Magnetic susceptibility and magnetization data were fit by using a nonlinear least-squares curve-fitting program, DSTEPIT.[41] This FORTRAN program was linked to subroutines that set up a 125 × 125 spin Hamiltonian matrix for the determination of the energy levels by matrix diagonalization with the EISPACK[42] subroutines and calculation of the powder susceptibility and magnetization data by using Van Vleck's equations.[28,40,43] Labeling of the spin sites Fe_{1-3} and associated exchange coupling parameters is as indicated in Figure 2. The general spin Hamiltonian in eq 1 was

$$\mathcal{H} = \sum S_i \cdot J_{ij} \cdot S_j \; (i = 1-3; j = 2, 3; j \neq i) + \sum S_i \cdot \mathbf{D}_i \cdot S_i \; (i = 1-3) + \sum \mathbf{B} \cdot \mathbf{g}_i \cdot S_i \; (i = 1-3) \quad (1)$$

employed, incorporating the exchange coupling, zero-field splitting, and electronic Zeeman terms. As suggested by Griffith,[44] J, rather than $-J$, $-2J$, or $2J$, was employed as the exchange coupling parameter. Several simplifications in each term were made so as to render the fitting procedure more tractable. First, an isotropic J was used; dipolar exchange interactions between spin sites were not taken into account.[45] Second, the electronic coordinate system for each of the three spin sites was assumed to have the same orientation (D_i, g_i, i = 1, 3 collinear), and only axial zero-field splitting was considered for each spin site (E_i

(40) (a) O'Connor, C. J. *Prog. Inorg. Chem.* **1982**, *29*, 203−283. (b) Carlin, R. L. *Magnetochemistry*; Springer-Verlag: New York, 1986.
(41) Program 66, Quantum Chemistry Program Exchange, Indiana University, Bloomington, IN.
(42) Garbow, B. S. Applied Mathematics Division, Argonne National Laboratory, Argonne, IL.
(43) Drago, R. S. *Physical Methods for Chemists*, 2nd ed.; Saunders: Orlando, FL, 1992; pp 473−483.
(44) Griffith, J. S. *Struct. Bonding (Berlin)* **1972**, *10*, 87−126.
(45) Weltner, W., Jr. *Magnetic Atoms and Molecules*; Dover: New York, 1989; pp 304−312.

Table 4. Positional Parameters and B(eq) for $[Fe_3(O_2CPh)_6(^iPrOx)_2]$ (**5**)[a]

atom	x	y	z	B(eq)[b]	atom	x	y	z	B(eq)[b]
Fe(1)	0.8966(1)	0.16944(8)	0.44753(7)	1.71(8)	C(24)	0.902(1)	−0.2311(7)	0.6999(6)	3.2(3)
Fe(2)	0.8854(1)	−0.00369(9)	0.49971(8)	1.60(7)	C(25)	0.810(1)	−0.2676(8)	0.6952(7)	4.6(4)
Fe(3)	0.8998(1)	−0.18409(8)	0.54584(8)	1.85(8)	C(26)	0.932(1)	−0.2271(9)	0.7621(7)	4.9(4)
O(1)	0.9816(7)	0.3520(5)	0.3568(4)	3.3(5)	C(27)	0.8670(9)	0.1564(6)	0.5563(6)	2.1(2)
O(2)	0.6939(6)	0.3262(5)	0.4082(4)	3.0(5)	C(28)	0.8407(8)	0.1545(6)	0.6192(5)	1.7(2)
O(3)	0.7880(6)	−0.3844(4)	0.4895(4)	2.8(4)	C(29)	0.854(1)	0.2122(7)	0.6549(6)	2.8(3)
O(4)	0.9833(6)	−0.3780(4)	0.6205(4)	2.4(4)	C(30)	0.823(1)	0.2108(7)	0.7118(6)	3.3(3)
O(5)	0.8531(6)	0.1049(4)	0.5234(4)	2.1(4)	C(31)	0.779(1)	0.1526(7)	0.7316(6)	3.2(3)
O(6)	0.8993(6)	0.2126(4)	0.5355(3)	2.1(4)	C(32)	0.764(1)	0.0953(7)	0.6979(7)	3.5(3)
O(7)	1.0059(6)	0.0187(4)	0.4543(4)	2.2(4)	C(33)	0.796(1)	0.0947(7)	0.6412(6)	2.7(3)
O(8)	1.0300(5)	0.1336(4)	0.4615(4)	2.3(4)	C(34)	1.055(1)	0.0711(6)	0.4520(6)	2.1(2)
O(9)	0.7955(6)	0.0123(4)	0.4298(4)	2.1(4)	C(35)	1.1525(8)	0.0647(6)	0.4343(5)	1.4(2)
O(10)	0.8535(6)	0.1056(4)	0.3842(4)	2.0(4)	C(36)	1.215(1)	0.1174(7)	0.4394(6)	2.6(3)
O(11)	0.9063(5)	−0.1122(4)	0.4728(3)	1.9(4)	C(37)	1.304(1)	0.1077(7)	0.4201(6)	3.1(3)
O(12)	0.9984(6)	−0.2027(4)	0.4710(4)	2.5(4)	C(38)	1.330(1)	0.0454(8)	0.3975(7)	3.9(3)
O(13)	0.9657(6)	−0.0127(5)	0.5731(4)	2.6(4)	C(39)	1.272(1)	−0.0072(8)	0.3929(7)	3.8(3)
O(14)	0.9940(6)	−0.1244(4)	0.5934(4)	2.3(4)	C(40)	1.181(1)	0.0004(7)	0.4100(6)	2.7(3)
O(15)	0.7707(6)	−0.0383(4)	0.5462(4)	2.3(4)	C(41)	0.8009(9)	0.0543(6)	0.3877(5)	1.6(2)
O(16)	0.7803(6)	−0.1481(4)	0.5795(4)	2.4(4)	C(42)	0.733(1)	0.0450(6)	0.3384(6)	2.1(2)
N(1)	0.9567(7)	0.2462(5)	0.3931(4)	1.8(5)	C(43)	0.651(1)	0.0113(7)	0.3484(6)	3.0(3)
N(2)	0.7705(7)	0.2305(5)	0.4325(4)	1.6(5)	C(44)	0.588(1)	0.0093(7)	0.3023(6)	3.4(3)
N(3)	0.8144(7)	−0.2702(5)	0.5038(5)	2.2(5)	C(45)	0.611(1)	0.0378(8)	0.2494(7)	4.3(3)
N(4)	0.9488(8)	−0.2669(5)	0.5998(4)	2.2(5)	C(46)	0.693(1)	0.0686(8)	0.2394(7)	3.8(3)
C(1)	0.855(1)	0.3411(7)	0.4199(6)	3.1(3)	C(47)	0.752(1)	0.0733(7)	0.2855(6)	3.1(3)
C(2)	0.935(1)	0.3090(7)	0.3898(6)	2.3(3)	C(48)	0.9671(9)	−0.1499(6)	0.4453(6)	2.2(2)
C(3)	1.055(1)	0.3099(7)	0.3318(6)	3.0(3)	C(49)	0.994(1)	−0.1293(7)	0.3857(6)	2.6(3)
C(4)	1.039(1)	0.2378(7)	0.3550(6)	2.7(3)	C(50)	0.942(1)	−0.0837(7)	0.3553(6)	3.0(3)
C(5)	1.021(1)	0.1816(7)	0.3099(6)	3.0(3)	C(51)	0.969(1)	−0.0606(8)	0.3014(7)	3.7(3)
C(6)	0.944(1)	0.2010(8)	0.2694(6)	3.3(3)	C(52)	1.047(1)	−0.0852(8)	0.2769(7)	4.0(3)
C(7)	1.110(1)	0.1674(8)	0.2769(7)	4.6(4)	C(53)	1.100(1)	−0.1324(7)	0.3075(6)	3.5(3)
C(8)	0.773(1)	0.2944(7)	0.4222(6)	2.4(3)	C(54)	1.074(1)	−0.1563(7)	0.3622(6)	2.5(3)
C(9)	0.623(1)	0.2753(7)	0.4170(6)	3.1(3)	C(55)	1.0058(9)	−0.0588(6)	0.5989(5)	1.7(2)
C(10)	0.675(1)	0.2064(7)	0.4207(5)	2.2(3)	C(56)	1.0772(8)	−0.0374(6)	0.6440(5)	1.5(2)
C(11)	0.640(1)	0.1550(6)	0.4665(5)	2.3(3)	C(57)	1.103(1)	0.0304(7)	0.6475(7)	3.9(3)
C(12)	0.544(1)	0.1315(8)	0.4503(7)	3.9(3)	C(58)	1.169(1)	0.0505(8)	0.6887(7)	4.5(4)
C(13)	0.642(1)	0.1853(7)	0.5278(6)	3.1(3)	C(59)	1.206(1)	0.003(1)	0.7256(7)	4.4(4)
C(14)	0.9383(9)	−0.3551(6)	0.5222(5)	2.0(2)	C(60)	1.181(1)	−0.0651(9)	0.7211(7)	4.3(4)
C(15)	0.8449(9)	−0.3314(6)	0.5035(5)	1.8(2)	C(61)	1.118(1)	−0.0858(7)	0.6791(6)	3.3(3)
C(16)	0.698(1)	−0.3532(7)	0.4825(6)	2.9(3)	C(62)	0.741(1)	−0.0914(6)	0.5711(5)	2.2(3)
C(17)	0.717(1)	−0.2749(6)	0.4839(5)	2.4(3)	C(63)	0.640(1)	−0.0870(6)	0.5880(6)	2.2(2)
C(18)	0.703(1)	−0.2382(6)	0.4257(5)	2.1(2)	C(64)	0.594(1)	−0.0262(8)	0.5835(7)	4.4(4)
C(19)	0.770(1)	−0.2632(7)	0.3794(6)	3.2(3)	C(65)	0.501(1)	−0.0230(8)	0.6006(7)	4.4(4)
C(20)	0.697(1)	−0.1605(8)	0.4304(6)	3.7(3)	C(66)	0.459(1)	−0.0815(8)	0.6204(7)	4.0(3)
C(21)	0.9565(8)	−0.3286(6)	0.5822(5)	1.7(2)	C(67)	0.506(1)	−0.1404(7)	0.6267(6)	3.1(3)
C(22)	0.997(1)	−0.3410(7)	0.6763(6)	3.0(3)	C(68)	0.596(1)	−0.1450(6)	0.6105(5)	2.4(2)
C(23)	0.975(1)	−0.2659(7)	0.6617(6)	2.4(3)					

[a] For atom-labeling scheme, see Figure 4. Estimated standard deviations in the least significant figure are given in parentheses. [b] $B(\text{eq}) = {}^8/_3\pi^2(U_{11}(aa^*)^2 + U_{22}(bb^*)^2 + U_{33}(cc^*)^2 + 2U_{12}aa^*bb^* \cos\gamma + 2U_{13}aa^*cc^* \cos\beta + 2U_{23}bb^*cc^* \cos\alpha)$.

$= 0$; $i = 1-3$). Third, in accord with the previous simplification, the **g** tensor was constrained to be axially symmetric ($g_{iy} = g_{ix}$; $i = 1-3$). These same approximations were made previously in a study of a linear Ni(II) trimer.[46] Finally, fourth-order zero-field splitting terms were ignored, although these terms (e.g., F) can be present for $S \geq 2$.[47] Simulations were also performed without zero-field splitting ($D_i = 0$) and with only an isotropic single-ion g value, which we refer to as the "Kambé-type" model.[27]

Constraints were imposed on the fitting procedure that were based on the molecular symmetry. Individual magnetic parameters for the terminal ferrous sites were set to be equivalent: $D_1 = D_3$ and $g_{l1} = g_{l3}$; $l = x, y, z$. Exchange couplings between the terminal and middle ferrous sites were held to be equal: $J_{12} = J_{23}$. In general, the terminal−terminal exchange coupling was fixed at zero ($J_{13} = 0$), although this restriction is not symmetry imposed. The effect of $J_{13} \neq 0$ was explored in fits of the susceptibility data (see Results and Discussion). Calculations were performed on an IBM RS/6000 computer maintained by the Department of Chemistry, Northwestern University.

EPR Theory. A computer program employing full-matrix diagonalization, similar to the one employed in the magnetic data fitting, was used to generate EPR transition energies and probabilities. The latter were obtained by first determining magnetic dipole allowedness from the eigenvectors and then applying the resonance condition with the microwave quantum (at X-band, ≈ 0.3 cm^{-1}). No attempt was made to generate powder patterns. Instead, three "single-crystal" calculations were made with $B_0 = B_x$, B_y, and B_z, successively. No iterative spectral simulations were performed. The function of the program was to confirm that the observed EPR signals could arise from the trinuclear system with the parameters determined from fitting of the magnetic data.

Results and Discussion

Syntheses. The ligand $PheMe_3Eda$ was originally prepared to provide a bidentate nitrogen donor ligand with a pendant phenol for use in generating a model for the active site of the ribonucleotide reductase R2 protein. Such a model, comprising an oxo-bridged diiron(III) unit and a noncoordinated phenoxyl radical moiety, was made by using BIDPhEH, as reported previously.[31] Both BIDPhEH and $PheMe_3Eda$ also afforded linear, carboxylate-bridged trinuclear Fe(II) complexes, analogous to $[Fe_3(OAc)_6(BIPhMe)_2]$.[29] These compounds allowed us to expand this class of molecules and to compare in detail

(46) Boyd, P. D. W.; Martin, R. L. *J. Chem. Soc., Dalton Trans.* **1979**, 92−95.
(47) Abragam, A.; Bleaney, B. *Electron Paramagnetic Resonance of Transition Ions*; Dover: New York, 1986; pp 436−446.

Table 5. Positional Parameters and *B*(eq) Values for $[Fe_3(O_2CPh)_6(PheMe_3Eda)_2]$ (**6**)[a]

atom	*x*	*y*	*z*	*B*(eq)[b]
Fe(1)	0.19954(6)	0.09627(2)	1.00536(4)	1.62(3)
Fe(2)	0	0	1.0000	1.64(4)
O(1)	0.1835(3)	0.10434(9)	1.1592(2)	2.0(1)
O(2)	0.1521(3)	0.0416(1)	1.0906(2)	1.9(1)
O(3)	0.1165(3)	0.0021(1)	0.8937(2)	2.4(1)
O(4)	0.2099(4)	0.0665(1)	0.8809(2)	2.7(1)
O(5)	−0.0015(3)	0.1137(1)	0.9734(2)	2.2(1)
O(6)	−0.1160(3)	0.0528(1)	0.9398(2)	2.4(1)
O(7)	0.1711(3)	0.1803(1)	0.2502(2)	2.0(1)
N(1)	0.4273(4)	0.0902(1)	1.0527(3)	2.4(2)
N(2)	0.2590(4)	0.1625(1)	0.9713(3)	1.8(1)
C(1)	0.4826(5)	0.1280(2)	1.0121(4)	2.8(2)
C(2)	0.4002(5)	0.1672(2)	1.0219(4)	2.7(2)
C(3)	0.4757(6)	0.0904(2)	1.1564(4)	4.4(3)
C(4)	0.4810(6)	0.0513(2)	1.0133(5)	4.8(3)
C(5)	0.1757(5)	0.1956(2)	1.0070(3)	2.5(2)
C(6)	0.2557(5)	0.1695(1)	0.8675(3)	2.1(2)
C(7)	0.1181(5)	0.1674(1)	0.8022(3)	2.2(2)
C(8)	0.1422(5)	0.1722(2)	0.6989(3)	2.2(2)
C(9)	0.0186(5)	0.1742(1)	0.6183(3)	1.9(2)
C(10)	−0.0634(6)	0.1337(2)	0.6195(4)	3.6(3)
C(11)	−0.0701(6)	0.2128(2)	0.6341(3)	3.5(2)
C(12)	0.0616(5)	0.1785(1)	0.5202(3)	1.7(2)
C(13)	0.1960(5)	0.1806(1)	0.5104(3)	2.0(2)
C(14)	0.2362(4)	0.1822(1)	0.4224(3)	1.7(2)
C(15)	0.1344(5)	0.1814(1)	0.3402(3)	1.7(2)
C(16)	−0.0026(4)	0.1828(1)	0.3461(3)	1.7(2)
C(17)	−0.0346(5)	0.1809(1)	0.4364(3)	1.9(2)
C(18)	0.3872(5)	0.1823(2)	0.4163(3)	2.1(2)
C(19)	0.4763(5)	0.1879(2)	0.5143(4)	3.7(3)
C(20)	0.4242(5)	0.1398(2)	0.3770(4)	3.3(2)
C(21)	0.4192(5)	0.2188(2)	0.3536(4)	3.2(2)
C(22)	−0.1151(5)	0.1856(1)	0.2557(3)	2.0(2)
C(23)	−0.0915(5)	0.2252(2)	0.1974(4)	2.9(2)
C(24)	−0.2547(5)	0.1905(2)	0.2813(4)	3.1(2)
C(25)	−0.1181(5)	0.1460(2)	0.1937(4)	2.8(2)
C(26)	0.1593(4)	0.0644(1)	1.1647(3)	1.7(2)
C(27)	0.1470(5)	0.0447(1)	1.2576(3)	1.9(2)
C(28)	0.1364(6)	0.0698(2)	1.3358(3)	2.7(2)
C(29)	0.1275(6)	0.0502(2)	1.4229(4)	3.8(3)
C(30)	0.1321(6)	0.0065(2)	1.4304(4)	4.0(3)
C(31)	0.1442(6)	−0.0178(2)	1.3537(4)	3.9(3)
C(32)	0.1526(5)	0.0004(1)	1.2658(4)	2.6(2)
C(33)	0.1857(5)	0.0275(2)	0.8559(3)	2.2(2)
C(34)	0.2465(5)	0.0118(1)	0.7740(3)	2.2(2)
C(35)	0.2129(5)	−0.0280(2)	0.7351(3)	2.7(2)
C(36)	0.2742(6)	−0.0442(2)	0.6652(4)	3.4(2)
C(37)	0.3722(7)	−0.0219(2)	0.6324(4)	4.4(3)
C(38)	0.4070(9)	0.0176(3)	0.6702(5)	7.0(4)
C(39)	0.3428(8)	0.0347(2)	0.7400(5)	5.7(4)
C(40)	−0.1038(5)	0.0924(1)	0.9372(3)	1.8(2)
C(41)	−0.2198(5)	0.1181(1)	0.8833(3)	1.9(2)
C(42)	−0.3188(5)	0.0986(1)	0.8148(4)	2.4(2)
C(43)	−0.4155(5)	0.1229(2)	0.7585(4)	2.9(2)
C(44)	−0.4222(5)	0.1664(2)	0.7742(4)	3.2(2)
C(45)	−0.3296(5)	0.1855(2)	0.8448(4)	3.3(2)
C(46)	−0.2275(5)	0.1613(2)	0.8983(4)	2.4(2)

[a] For atom-labeling scheme, see Figure S8. Estimated standard deviations in the least significant figure are given in parentheses. [b] $B(\text{eq}) = {}^8/_3\pi^2(U_{11}(aa^*)^2 + U_{22}(bb^*)^2 + U_{33}(cc^*)^2 + 2U_{12}aa^*bb^* \cos\gamma + 2U_{13}aa^*cc^* \cos\beta + 2U_{23}bb^*cc^* \cos\alpha)$.

the magnetic properties of a series of similar, but structurally and magnetochemically distinguishable, trinuclear ferrous species.

Reaction of equimolar amounts of 2,6-di-*tert*-butylphenol, 4-chlorobutyryl chloride, and $AlCl_3$ afforded the ketone (3,5-di-*tert*-butyl-4-hydroxyphenyl)-4-chlorobutanone (**2a**) in 61% yield after purification by column chromatography. A previous report demonstrated that ketones can be dimethylated by using Me_2TiCl_2, prepared from Me_2Zn and $TiCl_4$, under very mild conditions.[48,49] This strategy was employed to obtain the methylated product **2b** from **2a** in 74% yield after purification by column chromatography. The final $PheMe_3Eda$ ligand was obtained by reaction of **2b** with *N,N,N'*-trimethylethylenediamine and isolated as an oil in 77% yield after vacuum distillation. These steps are summarized in Scheme 1.

Table 6. Selected Bond Lengths (Å) and Angles (deg) for $[Fe_3(OAc)_6(BIPhOH)_2]\cdot 2MeOH$ (**3**)[a]

(a) Distances			
Fe(1)−Fe(2)	3.4081(6)	Fe(1)−N(3)	2.147(4)
Fe(1)−O(1)	2.063(3)	Fe(2)−O(1)	2.198(3)
Fe(1)−O(4)	2.072(3)	Fe(2)−O(3)	2.045(3)
Fe(1)−O(6)	2.021(3)	Fe(2)−O(5)	2.168(3)
Fe(1)−N(1)	2.103(4)		
(b) Angles			
Fe(1)−O(1)−Fe(2)	106.2(1)	O(4)−Fe(1)−N(3)	176.0(1)
O(6)−Fe(1)−O(1)	115.6(1)	N(1)−Fe(1)−N(3)	84.3(1)
O(6)−Fe(1)−O(4)	92.8(1)	O(3)−Fe(2)−O(5)	93.0(1)
O(6)−Fe(1)−N(1)	117.7(1)	O(3)−Fe(2)−O(5)′	87.0(1)
O(6)−Fe(1)−N(3)	88.3(1)	O(3)−Fe(2)−O(1)	89.2(1)
O(1)−Fe(1)−O(4)	93.4(1)	O(3)−Fe(2)−O(1)′	90.8(1)
O(1)−Fe(1)−N(1)	126.0(1)	O(5)−Fe(2)−O(1)	91.7(1)
O(1)−Fe(1)−N(3)	89.6(1)	O(5)−Fe(2)−O(1)′	88.3(1)
O(4)−Fe(1)−N(1)	91.8(1)		

[a] For atom-labeling scheme, see Figure S7. Estimated standard deviations in the least significant figure are given in parentheses.

Table 7. Selected Bond Lengths (Å) and Angles (deg) for $[Fe_3(OAc)_6(BIDPhEH)_2]\cdot 4CH_3CN$ (**4**)[a]

(a) Distances			
Fe(1)−Fe(2)	3.282(1)	Fe(1)−N(3)	2.128(4)
Fe(1)−O(2)	2.045(3)	Fe(2)−O(2)	2.178(3)
Fe(1)−O(5)	2.043(4)	Fe(2)−O(4)	2.196(3)
Fe(1)−O(6)	2.126(3)	Fe(2)−O(7)	2.028(3)
Fe(1)−N(1)	2.070(4)		
(b) Angles			
Fe(1)−O(1)−Fe(2)	101.9(1)	O(6)−Fe(1)−N(3)	178.5(1)
O(2)−Fe(1)−O(5)	123.7(1)	N(1)−Fe(1)−N(3)	85.3(1)
O(2)−Fe(1)−O(6)	90.8(1)	O(2)−Fe(2)−O(4)	92.1(1)
O(2)−Fe(1)−N(1)	133.5(1)	O(2)−Fe(2)−O(4)′	87.9(1)
O(2)−Fe(1)−N(3)	90.0(1)	O(2)−Fe(2)−O(7)	90.7(1)
O(5)−Fe(1)−O(6)	89.9(1)	O(2)−Fe(2)−O(7)′	89.3(1)
O(5)−Fe(1)−N(1)	102.6(1)	O(4)−Fe(2)−O(7)	93.8(1)
O(5)−Fe(1)−N(3)	90.8(1)	O(4)−Fe(2)−O(7)′	86.2(1)
O(6)−Fe(1)−N(1)	93.3(1)		

[a] For atom-labeling scheme, see Figure 3. Estimated standard deviations in the least significant figure are given in parentheses.

Two facile synthetic routes were devised for preparing the five trinuclear ferrous complexes reported here. The first, described elsewhere for **1**[29] and employed in the syntheses of **3** and **4**, combines $Fe(OAc)_2$ with the bidentate nitrogen donor ligand in a 3:2 ratio. The same general procedure was used to obtain the related Mn(II) complex $[Mn_3(O_2CPh)_6(bpy)_2]$.[50] An analogous trinuclear V(II) complex, $[V_3(O_2CR)_6(TMEDA)_2]$ [R = Ph_2CH, $PhCH_2$; TMEDA = tetramethylethylenediamine], was prepared by treating $VCl_2(TMEDA)_2$ with neat carboxylic acid.[51] Crystallization of all three complexes in good yield was readily accomplished by vapor diffusion of the appropriate precipitating solvent. An alternative route, used for complexes **5** and **6**, combines $Fe(BF_4)_2\cdot 6H_2O$, the appropriate bidentate nitrogen donor ligand, and a 2- to 5-fold excess of sodium benzoate. The resulting trinuclear complexes are neutral and easily extracted into aromatic solvents, allowing for purification from unreacted carboxylate salts. Complexes **5** and **6** were crystallized in good yield as described for **1**, **3**, and **4**.

(48) Reetz, M. T.; Westermann, J. *J. Org. Chem.* **1983**, *48*, 254−255.
(49) Reetz, M. T.; Westermann, J.; Steinbach, R. *J. Chem. Soc., Chem. Commun.* **1981**, 237−239.
(50) Christou, G. *Acc. Chem. Res.* **1989**, *22*, 328−335.
(51) Edema, J. J. H.; Gambarotta, S.; Hao, S.; Bensimon, C. *Inorg. Chem.* **1991**, *30*, 2584−2586.

Table 8. Selected Bond Lengths (Å) and Angles (deg) for $[Fe_3(O_2CPh)_6(^tPrOx)_2]$ (**5**)[a]

(a) Distances

Fe(1)−Fe(2)	3.554(2)	Fe(2)−O(9)	2.106(8)
Fe(2)−Fe(3)	3.645(3)	Fe(2)−O(11)	2.205(8)
Fe(1)−O(5)	2.242(8)	Fe(2)−O(13)	2.070(9)
Fe(1)−O(6)	2.194(8)	Fe(2)−O(15)	2.105(8)
Fe(1)−O(8)	2.100(8)	Fe(3)−O(11)	2.183(8)
Fe(1)−O(10)	2.013(8)	Fe(3)−O(12)	2.282(9)
Fe(1)−N(1)	2.13(1)	Fe(3)−O(14)	2.107(9)
Fe(1)−N(2)	2.22(1)	Fe(3)−O(16)	2.040(9)
Fe(2)−O(5)	2.216(8)	Fe(3)−N(3)	2.29(1)
Fe(2)−O(7)	2.099(9)	Fe(3)−N(4)	2.15(1)

(b) Angles

Fe(1)−O(5)−Fe(2)	105.7(3)	O(7)−Fe(2)−O(13)	86.9(4)
Fe(2)−O(11)−Fe(3)	112.3(3)	O(9)−Fe(2)−O(15)	86.3(3)
O(5)−Fe(1)−O(6)	59.6(3)	O(11)−Fe(2)−O(13)	94.1(3)
O(5)−Fe(1)−O(8)	87.9(3)	O(11)−Fe(2)−O(15)	87.3(3)
O(5)−Fe(1)−O(10)	97.9(3)	O(13)−Fe(2)−O(15)	90.7(4)
O(5)−Fe(1)−N(1)	164.5(3)	O(7)−Fe(2)−O(15)	173.2(3)
O(6)−Fe(1)−N(2)	100.3(3)	O(9)−Fe(2)−O(11)	90.6(3)
O(6)−Fe(1)−O(8)	88.1(3)	O(9)−Fe(2)−O(13)	174.3(4)
O(6)−Fe(1)−O(10)	155.4(3)	O(11)−Fe(3)−O(12)	59.2(3)
O(6)−Fe(1)−N(1)	105.9(3)	O(11)−Fe(3)−O(14)	91.5(3)
O(6)−Fe(1)−N(2)	87.6(3)	O(11)−Fe(3)−O(16)	96.7(3)
O(8)−Fe(1)−O(10)	101.7(3)	O(11)−Fe(3)−N(3)	99.1(3)
O(8)−Fe(1)−N(1)	86.2(4)	O(11)−Fe(3)−N(4)	154.7(4)
O(8)−Fe(1)−N(2)	167.2(3)	O(12)−Fe(3)−O(14)	93.6(3)
O(10)−Fe(1)−N(1)	97.3(4)	O(12)−Fe(3)−O(16)	152.6(3)
O(10)−Fe(1)−N(2)	87.0(3)	O(12)−Fe(3)−N(3)	85.0(3)
N(1)−Fe(1)−N(2)	83.3(4)	O(12)−Fe(3)−N(4)	96.2(4)
O(5)−Fe(2)−O(7)	96.3(3)	O(14)−Fe(3)−O(16)	100.4(4)
O(5)−Fe(2)−O(9)	85.2(3)	O(14)−Fe(3)−N(3)	166.7(4)
O(5)−Fe(2)−O(11)	175.2(3)	O(14)−Fe(3)−N(4)	83.4(4)
O(5)−Fe(2)−O(13)	90.0(3)	O(16)−Fe(3)−N(3)	86.4(4)
O(5)−Fe(2)−O(15)	90.1(3)	O(16)−Fe(3)−N(4)	108.7(4)
O(7)−Fe(2)−O(9)	96.6(3)	N(3)−Fe(3)−N(4)	83.7(4)
O(7)−Fe(2)−O(11)	86.5(3)		

[a] For atom-labeling scheme, see Figure 4. Estimated standard deviations in the least significant figure are given in parentheses.

Table 9. Selected Bond Lengths (Å) and Angles (deg) for $[Fe_3(O_2CPh)_6(PheMe_3Eda)_2]$ (**6**)[a]

(a) Distances

Fe(1)−Fe(2)	3.6263(6)	Fe(1)−N(1)	2.284(4)
Fe(1)−O(1)	2.241(3)	Fe(1)−N(2)	2.241(4)
Fe(1)−O(2)	2.206(3)	Fe(2)−O(2)	2.234(3)
Fe(1)−O(4)	2.023(3)	Fe(2)−O(3)	2.086(3)
Fe(1)−O(5)	2.072(3)	Fe(2)−O(6)	2.117(3)

(b) Angles

Fe(1)−O(2)−Fe(2)	109.5(1)	O(4)−Fe(1)−N(1)	90.4(1)
O(1)−Fe(1)−O(2)	59.2(1)	O(4)−Fe(1)−N(2)	100.3(1)
O(1)−Fe(1)−O(4)	159.0(1)	O(5)−Fe(2)−N(1)	168.7(1)
O(1)−Fe(1)−O(5)	86.5(1)	O(5)−Fe(2)−N(2)	90.0(1)
O(1)−Fe(1)−N(1)	88.5(1)	N(1)−Fe(2)−N(2)	81.0(1)
O(1)−Fe(1)−N(2)	100.2(1)	O(2)−Fe(2)−O(3)	88.8(1)
O(2)−Fe(1)−N(4)	100.1(1)	O(2)−Fe(2)−O(3)′	91.2(1)
O(2)−Fe(1)−O(5)	91.2(1)	O(2)−Fe(2)−O(6)	92.6(1)
O(2)−Fe(1)−N(1)	94.8(1)	O(2)−Fe(2)−O(6)′	87.4(1)
O(2)−Fe(1)−N(2)	159.2(1)	O(3)−Fe(2)−O(6)	91.5(1)
O(4)−Fe(1)−O(5)	97.9(1)	O(3)−Fe(2)−O(6)′	88.5(1)

[a] For atom-labeling scheme, see Figure S8. Estimated standard deviations in the least significant figure are given in parentheses.

Molecular Structures. A detailed description of the structure shared by the five trinuclear complexes has been presented previously for complex **1**[29] and this class of compounds in general[52] and will not be reiterated here. Instead we highlight geometric parameters that are useful in understanding their magnetic properties. Compounds **3** (supplementary Figure S7), **4** (Figure 3), **5** (Figure 4) and **6** (supplementary Figure S8) have

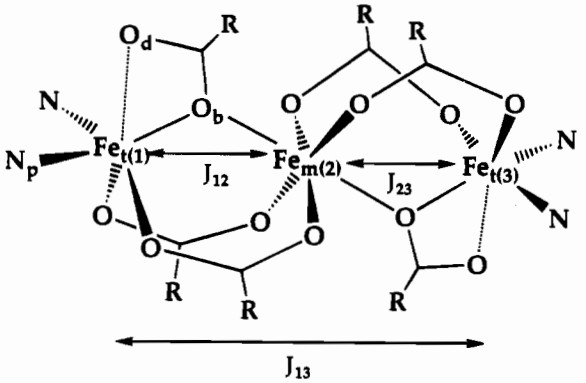

Figure 2. Generalized structure of the triiron(II) complexes.

a linear, trinuclear structure with a total of six bridging carboxylate ligands, four of which coordinate in a bidentate fashion through both oxygen atoms. The remaining two carboxylate ligands use a single oxygen atom to bridge two metal centers, leaving the remaining oxygen atom of this ligand available to coordinate to the nearest terminal iron atom. The bidentate nitrogen donor ligands cap the two ends of the trinuclear structure through binding to a terminal metal atom. A generalized depiction of these structural features is provided in Figure 2, and a comparison of selected bond distances and angles for compounds **1** and **3**−**6** is provided in Table 10.

The most striking difference among the structures of the five complexes is the Fe_t-O_d distance, which allows for their division into two classes. One class, comprising compounds **1**, **3**, and **4**, exhibits relatively weak bonding between O_d, the dangling oxygen atom, and Fe_t, the terminal metal atom, as revealed by the long $Fe_t\cdots O_d$ distances of 3.0 Å. The other consists of compounds **5** and **6**, which have much shorter distances, $Fe_t-O_d \approx 2.2$ Å, signifying coordination of the carboxylate oxygen atom. The movement of this atom toward the terminal iron atom in these two complexes pulls the bridging oxygen atom, O_b, away from Fe_m and additionally lengthens the Fe_t-O_b bond by as much as 0.21 Å compared to the Fe_t-O_b distances in the first group of complexes (see Table 10). Such a structural change, termed the "carboxylate shift," also occurs in metalloproteins and has been fully described elsewhere.[52]

The average Fe_t-N distance is significantly longer (0.1 Å) for both **5** and **6**, consistent with the higher coordination number of the terminal iron atoms in these complexes. The Fe_t atoms in both **5** and **6** exhibit geometries much nearer ideal octahedral symmetry than in **1**, **3**, or **4**, as reflected by the $N_p-Fe_t-O_b$ angles, illustrated in Figure 2 and listed in Table 10. The widening of this angle is another consequence of the short Fe_t-O_d distance. The difference in the Fe_t-O_d distances correlate well with a significant change in the magnetochemical properties of the two types of complexes, as discussed below.

Magnetic Susceptibility Studies. Temperature-dependent molar susceptibility data previously reported for **1** were erroneously high owing to torquing of the crystallites in the applied field. Such reorientation phenomena have been observed before, including in some Fe(II) systems.[53−56] Further experiments exploring the effects of the applied field on the magnetic susceptibility confirmed that partial torquing of the crystallites was definitely occurring in the original measurement.[57] The

(52) Rardin, R. L.; Tolman, W. B.; Lippard, S. J. *New. J. Chem.* **1991**, *15*, 417−430.

(53) Behere, D. V.; Date, S. K.; Mitra, S. *Chem. Phys. Lett.* **1979**, *68*, 544−548.

(54) Kennedy, B. J.; Murray, K. S. *Inorg. Chem.* **1985**, *24*, 1552−1557.

(55) Charron, F. F., Jr.; Reiff, W. M. *Inorg. Chem.* **1986**, *25*, 2786−2790.

(56) Sessoli, R.; Tsai, H.-L.; Schake, A. R.; Wang, S.; Vincent, J. B.; Folting, K.; Gatteschi, D.; Christou, G.; Hendrickson, D. N. *J. Am. Chem. Soc.* **1993**, *115*, 1804−1816.

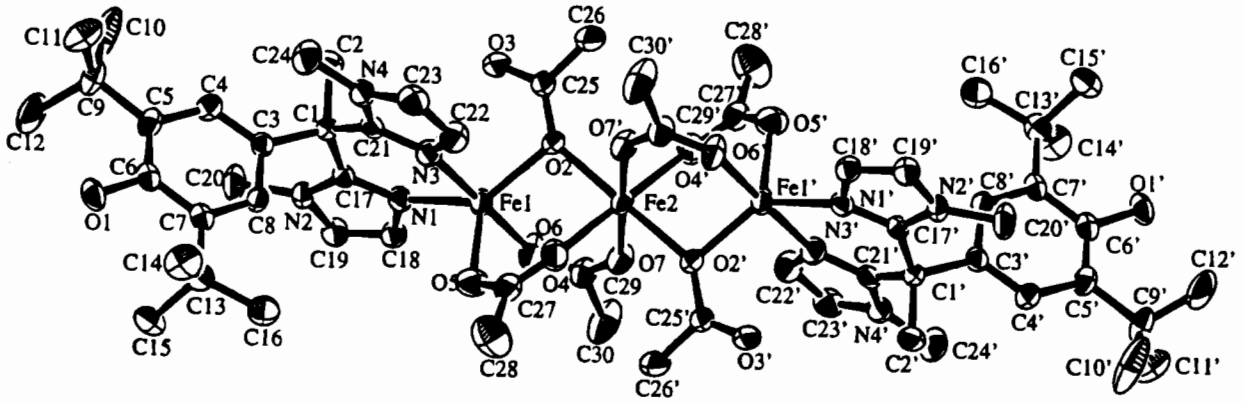

Figure 3. ORTEP diagram of $[Fe_3(OAc)_6(BIDPhEH)_2]$ (**4**) showing 50% probability thermal ellipsoids. Hydrogen atoms have been omitted for clarity.

Scheme 1

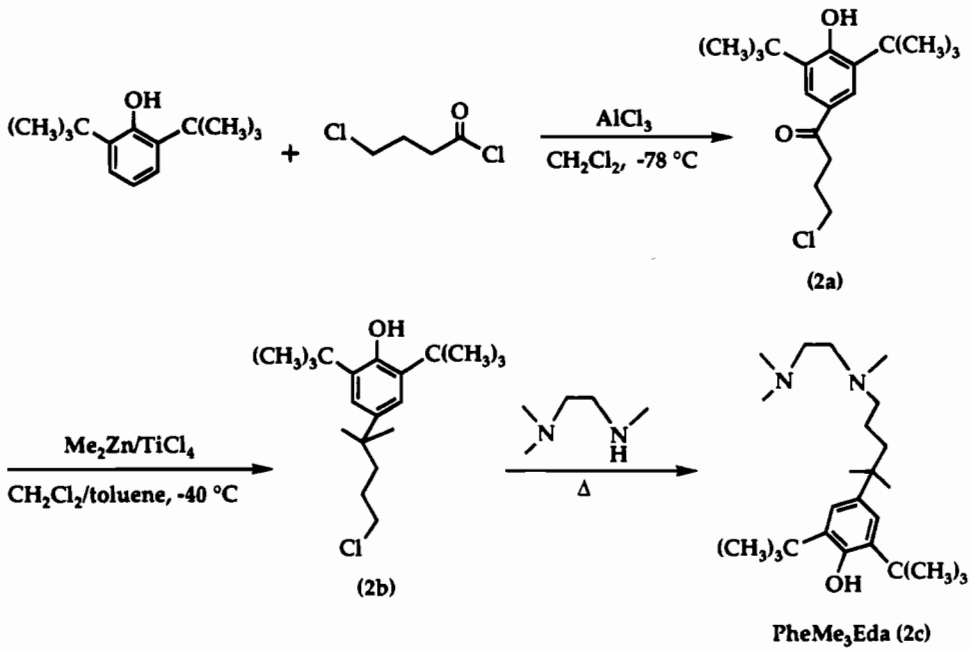

original measurement, made at 3 kG, correctly revealed ferromagnetic coupling for **1**, but at 4 K the effective magnetic moment derived from the low-temperature data was 17.3 μ_B. The theoretical value of μ_{eff} for three fully ferromagnetically coupled Fe(II) atoms having $S = 6$ is 12.96 μ_B for $g = 2.0$ (Table 11). Intermolecular interactions were suggested as the possible cause of the unexpectedly high moment. When the data were measured at a much lower field of 100 G to avoid possible reorientation of the crystallites, ferromagnetic coupling was maintained but μ_{eff} was 12.7 μ_B at 6 K, a value consistent with an $S = 6$ ground state.

Plots of the effective magnetic moment versus temperature for **1**, **3**, and **4** are shown in Figures 5, S1 (supplementary), and S3 (supplementary), respectively. Above 200 K, all three of these complexes exhibit effective magnetic moments close to the theoretical value of 8.49 μ_B expected for three independent $S = 2$ ferrous ions with $g = 2.0$ (Table 11). The steep rise in the effective moment is characteristic of ferromagnetic coupling below 80 K for all three complexes. As for **1**, the BIPhOH and BIDPhEH complexes have μ_{eff} values approaching the 12.96 μ_B theoretical value for an $S = 6$ system at low temperatures, with $\mu_{eff} = 11.7$ μ_B at 7 K for **3** and $\mu_{eff} = 12.3$ μ_B at 5 K for complex **4**.

(57) Goldberg, D. P. Ph.D. Thesis, Massachusetts Institute of Technology, 1994.

The temperature dependence of μ_{eff} for complexes **5** and **6** is shown in Figures 6 and S5 (supplementary), respectively. Near 300 K, the effective moments are 9.52 and 9.50 μ_B for the ^{i}PrOx and PheMe$_3$Eda complexes, respectively. These values are similar to the spin-only value expected for three isolated $S = 2$ ions near 300 K, described above. As the temperature decreases, the effective moments also decrease, revealing antiferromagnetic coupling for both **5** and **6**. The ground state for full antiferromagnetic coupling and $S = 2$ has a theoretical spin-only value of 4.90 μ_B assuming $g = 2.0$. The ^{i}PrOx and PheMe$_3$Eda complexes have μ_{eff} values of 6.52 and 6.74 μ_B at 5 K, approaching this value.

Magnetization Studies. Plots of the reduced magnetization, $M/N\mu_B$, vs field at 2 K for complexes **1**, **3**, and **4** are included as insets in Figures 5, S1, and S3, respectively. In all of these ferromagnetically coupled complexes, a steep rise occurs in the reduced magnetization at low fields, followed by a slow, steady increase up to the maximum field of 200 kOe. Both **1** and **3** reach 11.5 μ_B in reduced magnetization at 200 kOe, and compound **4** obtains a value of 10.9 μ_B at this field. The theoretical value of $M/N\mu_B$ is 12.0 μ_B for an $S = 6$ ground state, assuming $g = 2.0$, close to the experimental values of the reduced magnetization for **1**, **3**, and **4**. None of the curves exhibits a plateau region that would be expected if the

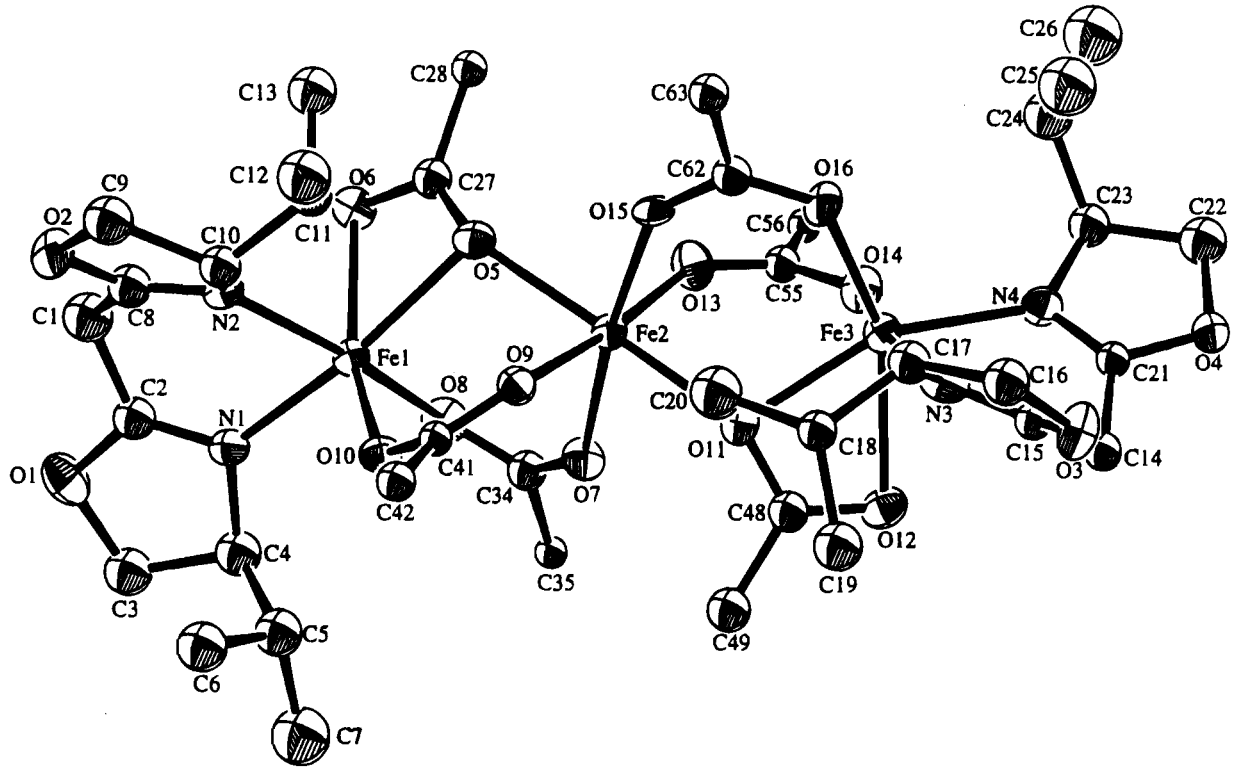

Figure 4. ORTEP diagram of $[Fe_3(O_2CPh)_6(^iPrOx)_2]$ (**5**) showing 50% probability thermal ellipsoids. All benzoate ring carbon atoms, except for the site of carboxylate attachment, and hydrogen atoms have been omitted removed for clarity.

Table 10. Selected Bond Distances (Å) and Angles (deg) for **1** and **3**–**6**[a]

complex	Fe–Fe	Fe_t–O_d	Fe_t–O_b	Fe_m–O_b	Fe_t–N_{ave}[b]	N_p–Fe–O_b	Fe_t–O_b–Fe_m
1	3.3251(9)	3.005(4)	2.027(3)	2.151(3)	2.11(2)	124.6(1)	105.4(1)
3	3.4081(6)	3.043(3)	2.063(3)	2.198(3)	2.13(3)	126.0(1)	106.2(1)
4	3.282(1)	3.03(1)	2.045(3)	2.178(3)	2.10(4)	133.5(1)	101.9(1)
5	3.554(2)	2.194(8)	2.242(8)	2.216(8)	2.18(6)	164.5(3)	105.7(3)
	3.645(3)	2.282(9)	2.183(8)	2.205(8)	2.22(10)	166.7(4)	112.3(3)
6	3.6263(6)	2.241(3)	2.206(3)	2.234(3)	2.26(3)	159.2(1)	109.5(1)

[a] See Figure 2 for definition of atom labels. [b] Values in parentheses are the standard deviations in the averaged metrical parameters.

Table 11. Summary of the Susceptibility Data for Complexes **1** and **3**–**6**

complex	μ_{eff} (μ_B) at min T[a]	μ_{eff} (μ_B) at max T[b]
calcd for **1**, **3**, **4**[c]	12.96	8.49
1	12.7	9.03
3	11.7	9.08
4	12.3	9.21
calcd for **5** and **6**[d]	4.90	8.48
5	6.52	9.52
6	6.74	9.50

[a] The minimum temperatures are 3–7 K. [b] The maximum temperatures are 280–300 K. [c] Calculated assuming $S = 6$, $g = 2.0$. [d] Calculated assuming $S = 2$, $g = 2.0$.

magnetization were saturated by the high fields. The slow approach of the reduced magnetization to the theoretical value reveals that a field of 200 kOe is not strong enough, even at these low temperatures, for the ferromagnetic ground state of these weakly-coupled complexes to be populated exclusively.

The antiferromagnetically coupled compounds **5** and **6** display a more gradual increase in $M/N\mu_B$ with increasing magnetic field, as indicated in the insets of Figures 6 and S5. An $S = 2$ ground state should give rise to an $M/N\mu_B$ value of 4.0 μ_B assuming $g = 2.0$. This increase in $M/N\mu_B$ above 4.4 μ_B occurs because the Zeeman term becomes more important as the field is increased (vide infra).

Theoretical Analysis of the Magnetization Data. We have performed least-squares fits of both the susceptibility and high-field magnetization data to eq 1 for all five complexes with the programs described in the Experimental Section. Given a problem of this complexity, the final parameters for an individual fit can be quite sensitive to their initial values, so

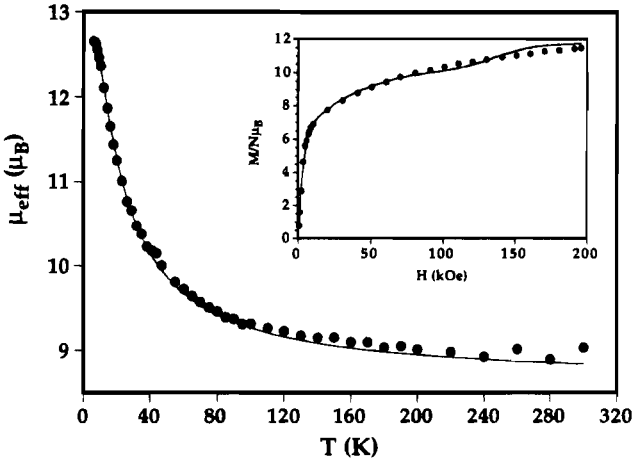

Figure 5. Plot of the effective magnetic moment vs temperature for a polycrystalline sample of **1**, together with the best fit (solid line, energies in cm^{-1}): $J = -3.97$, $D_{1,3} = -3.45$, $D_2 = -0.46$, $g_\perp(Fe_{1,3}) = 2.08$, $g_\parallel(Fe_{1,3}) = 1.98$, $g_\perp(Fe_2) = 1.99$, $g_\parallel(Fe_2) = 2.02$. Inset shows the plot of the reduced magnetization at 2 K vs field for a polycrystalline sample of **1**, together with the best fit (solid line, energies in cm^{-1}): $J = -4.00$ (fixed), $D_{1,3} = 6.45$, $D_2 = -10.1$, all g values fixed at 2.00.

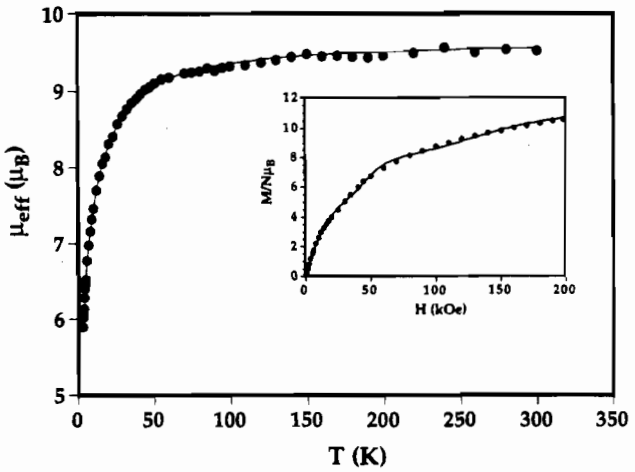

Figure 6. Plot of the effective magnetic moment vs temperature for a polycrystalline sample of **5**, together with the best fit (solid line, energies in cm^{-1}): $J = +0.99$, $D_{1,3} = 0.0$ (fixed), $D_2 = -11.5$, $g_\perp(Fe_{1,3}) = 2.14$, $g_\parallel(Fe_{1,3}) = 2.01$, $g_\perp(Fe_2) = 2.78$, $g_\parallel(Fe_2) = 2.13$. Inset shows the plot of the reduced magnetization at 2 K vs field for a polycrystalline sample of **5**, together with the best fit (solid line, energies in cm^{-1}): $J = +0.72$, $D_{1,3} = 0.0$ (fixed), $D_2 = -12.2$, $g_\perp(Fe_{1,3}) = 1.76$, $g_\parallel(Fe_{1,3}) = 1.42$, $g_\perp(Fe_2) = 3.03$, $g_\parallel(Fe_2) = 1.27$.

the following protocol was adopted for the susceptibility data. Initial values for the isotropic exchange coupling parameter ($J_{12} = J_{23}$; $J_{13} = 0$) were always fixed at zero, and the g values were always initiated at 2.0. Fits were performed by using initial values for D_i of 0, -10, and $+10$ cm^{-1} ($i = 1 = 3, 2$). This range approximately corresponds to the values reported previously for mononuclear ferrous systems (vide infra).[58,59] As described below, considerable difficulty was encountered in obtaining the absolute signs of D_i, although the magnitudes could be estimated. In fitting of the magnetization data, the same procedures were followed, although initial values of $D_i = \pm 10$ cm^{-1} were not used in all cases. Attempts were also made to fit the magnetization curves by using the Kambé-type model, the results of which were compared to the fits obtained from the more general model of eq 1.

In order to model completely a magnetic system having the complexity of the trinuclear ferrous systems described here, it would be necessary to measure the entire "magnetization surface", the three-dimensional space defined by temperature, external magnetic field, and the resulting magnetization. For a given compound, we have only two sections in this space, namely, variable-temperature susceptibility at one fixed field and variable-field magnetization at one fixed temperature. As a consequence, the best-fit parameters for the former may not agree with those of the latter. We therefore give "consensus" magnetic parameters, summarized in Table 12, that best account for both the susceptibility and magnetization data for all five complexes.

$[Fe_3(OAc)_6(BIPhMe)_2]$ (1). The fit of μ_{eff} vs temperature for this compound is shown in Figure 5. With an initial D_i of 0, the best-fit parameters were as follows (energies in cm^{-1}): $J = -3.97$, $D(Fe_{1,3}) = -3.45$, $D(Fe_2) = -0.46$, $g_\perp$ $(Fe_{1,3}) = 2.08$, $g_\parallel(Fe_{1,3}) = 1.98$, $g_\perp(Fe_2) = 1.99$, $g_\parallel(Fe_2) = 2.02$. The negative sign of J is consistent with ferromagnetic coupling. An initial D_i value of $\pm$ 10 cm^{-1} yielded similar magnetic parameters. Inclusion of J_{13} had little effect, giving $J_{12,23} = -4.62$ cm^{-1} and $J_{13} = +0.59$ cm^{-1}. Clearly, $J = -4 \pm 1$ cm^{-1} is indicated.

The Kambé-type model failed to fit the high-field magnetization data, but inclusion of zero-field splitting succeeded quite well, as shown in the inset of Figure 5. The fit parameters were as follows (energies in cm^{-1}): J fixed at -4.0, $D(Fe_{1,3}) = 6.45$, $D(Fe_2) = -10.1$, all g values fixed at 2.00. Allowing all the fixed parameters to vary led to a slightly improved fit, but with $J = -1.22$ cm^{-1}, and $D(Fe_{1,3}) = +10.1$ cm^{-1}, and $D(Fe_2) = -1.11$ cm^{-1}. Fixing the J values at -1.0 or -1.5 cm^{-1} led to a poor fit of the susceptibility data. Exact agreement of the magnetic parameters for the magnetization and susceptibility fits is simply not achievable, as indicated above. The consensus J value of -4 cm^{-1} fits the magnetization data adequately and the susceptibility data quite well.

$[Fe_3(OAc)_6(BIDPhEH)_2]$ (4). Figure S3 shows a representative fit of the μ_{eff} vs temperature curve for **4** employing the following parameters (energies in cm^{-1}): $J = -4.80$, $D(Fe_{1,3}) = 5.85$, $D(Fe_2) = 4.82$, $g_\perp(Fe_{1,3}) = 2.00$, $g_\parallel(Fe_{1,3}) = 2.38$, $g_\perp$-$(Fe_2) = 2.00$, $g_\parallel(Fe_2) = 2.02$. The fit used initial values for $D_i = 0$; initial values of ± 10 cm^{-1} yielded similar J and g values, and the final value for $D(Fe_2)$ remained near the initial one (e.g., $D(Fe_2) = 12.3$ cm^{-1}, $D(Fe_{1,3}) = 3.83$, and $J = -5.47$ cm^{-1}). Only an estimate of $|D_i| = 10 \pm 10$ cm^{-1} can be made with confidence from the susceptibility data. Magnetically isolated Fe(II) ions with distorted octahedral symmetry exhibit D values within this range, with $D \approx 10$ cm^{-1} being typical.[59] For example, magnetic studies of Fe^{2+} doped into $ZnSiF_6$ suggested $D = +10.9$ cm^{-1}, and EPR studies gave $D = -20.2$ cm^{-1}.[60] Magnetic studies in aqueous solution of Fe^{II}EDTA, a complex having a ligand set resembling those described here, gave $|D| = 9.1$ cm^{-1}; the EPR spectrum indicated a negative sign.[61] These examples serve to illustrate the difficulty of determining the sign of zfs parameters, even in mononuclear systems.

Values of 2.0−2.4 for g are as expected and arise from orbital angular momentum contributions. For d^6 ions in a cubic crystal field with significant spin−orbit coupling ($\lambda \approx 100$ cm^{-1}), an isotropic $g \leq 3.5$ is expected. Thus, for Fe(II) sites in MgO, $g = 3.428$ and, in NaF, $g = 3.420$.[47] In an axially distorted crystal field, as is the case with the present complexes, perturbation theory methods give $2.0 \leq g_\parallel, g_\perp \leq 2.4$.[60,62] For $Fe^{II}ZnSiF_6$, $g_\perp = 2.26$ and $g_\parallel = 2.38$ and for Fe^{II}EDTA, using the EPR results but removing the rhombic contribution, $g_\perp = 2.02$ and $g_\parallel = 2.20$.

The J value can be reported with more confidence as -5 ± 1 cm^{-1}. Even allowing exchange coupling between the terminal ferrous sites had little effect: $J_{12} = J_{23} = -5.18$ cm^{-1}; $J_{13} = +0.34$ cm^{-1}. The other parameters were similarly not substantially modified.

Inclusion of zero-field splitting led to reasonably good fits for the magnetization data of the BIDPhEH complex, but with $J \approx 0$. Fixing J at -5.0 cm^{-1}, the value derived from the fits of the susceptibility data, allowed for the successful fit of the high-field magnetization data, as shown in the inset of Figure S3.

$[Fe_3(OAc)_6(BIPhOH)_2]$ (3). A successful fit of the susceptibility data for **3** is given in Figure S1. The fits gave g values near 2.0 and a J value of -2.8 cm^{-1}, indicative of ferromagnetic coupling. The value for $D(Fe_{1,3})$ of -19.2 cm^{-1} seems unreasonably high, however. Alternative fitting attempts with varying initial D values yielded $D(Fe_{1,3})$ of ≈ 6 cm^{-1}, but the resulting value for $g_\parallel(Fe_2)$ was unreasonably low (<0.8). Other interactions such as nonaxial zfs terms, however, can manifest

(58) Hendrich, M. P.; Debrunner, P. G. *Biophys. J.* **1989**, *56*, 489−506.
(59) Tinkham, M. *Proc. R. Soc. London* **1956**, *A236*, 535−548.
(60) Rubins, R. S. *Proc. Phys. Soc.* **1962**, *80*, 244−247.
(61) See ref 58. These workers also determined $E = \pm 3$ cm^{-1} and -1 cm^{-1} based on EPR and magnetic susceptibility data, respectively.
(62) Hendrich, M. P.; Debrunner, P. G. *J. Magn. Reson.* **1988**, *78*, 133−141.

Table 12. Consensus Magnetic Parameters from Magnetic Susceptibility and Magnetization Data Fits[a]

complex	J[b]	$\|D\|(Fe_{1,3})$	$\|D\|(Fe_2)$	$g_\perp(Fe_{1,3})$	$g_\parallel(Fe_{1,3})$	$g_\perp(Fe_2)$	$g_\parallel(Fe_2)$
1	-4 ± 1	5 ± 5	5 ± 5	2.0 ± 0.1	2.0 ± 0.1	2.0 ± 0.1	2.0 ± 0.1
3[c]	$J_{12} = J_{23} = -2 \pm 2$; $J_{13} = 0.5 \pm 0.5$	6 ± 3	0 ± 5	≈ 2.0	≈ 2.0	≈ 2.0	≈ 2.0
4	-5 ± 1	5 ± 3	10 ± 10	2.0 ± 0.5	2.2 ± 0.2	2.0 ± 0.5	2.2 ± 0.2
5[c]	$+1.0 \pm 0.5$	0 ± 2	10 ± 5	≈ 2.0	≈ 2.0	≈ 2.0	≈ 2.0
6[c]	$+1.0 \pm 0.5$	0 ± 5	10 ± 5	≈ 2.0	≈ 2.0	≈ 2.0	≈ 2.0

[a] Energies are in cm^{-1}. See text for description of fitting procedure. [b] $\mathcal{H} = JS_i \cdot S_j$; $J = J_{12} = J_{23}$ and $J_{13} = 0$, except as noted otherwise. [c] Significant variability in the g values was obtained for these compounds (see text for details).

themselves in the apparent g value, leading to deviation of $g_\parallel$ from 2.0, even with spin−orbit coupling quenched.[63]

A possible explanation for the difficulty in fitting the susceptibility data is that **3** exhibits antiferromagnetic coupling between the terminal ferrous sites (i.e., $J_{13} > 0$). Inclusion of J_{13} led to g values near 2.0 and $D(Fe_{1,3})$ of ≈ 6 cm^{-1}, although the fit was relatively poor in the high-temperature region, where the molar susceptibility is quite low. Most of the fitting attempts for **3** consistently gave $D(Fe_2)$ values of very small magnitude, which may be related to the apparent relative importance of J_{13}. This result contrasts with those for **1** and **4**, for which the two zfs parameters $D(Fe_{1,3})$ and $D(Fe_2)$ were of comparable magnitude and inclusion of J_{13} had a negligible effect.

The magnetization data of **3** are given in the inset of Figure S1 together with the best fit. As was found with the susceptibility data fits, $D(Fe_2)$ consistently refined to nearly zero. Surprisingly, the magnetization fits yielded $J \approx 0$ as well, with or without variation of g. Ferromagnetic coupling between terminal and center spin sites combined with terminal−terminal antiferromagnetic coupling could lead to approximate cancellation of these effects. Although no dramatic improvement in the magnetization fits resulted from inclusion of J_{13}, as can be seen for the fit with $J_{13} = +0.96$ cm^{-1} in Figure S2, the fitting results as a whole suggest that this coupling may be significant for **3**. We conclude that net ferromagnetic coupling for the BIPhOH complex is significantly weaker than that for **1** or **4**, as a consequence either of an inherently smaller terminal-to-center coupling or of a competing antiferromagnetic interaction between terminal sites.

$[Fe_3(O_2CPh)_6(^iPrOx)_2]$ (5). The most reasonable fit to the susceptibility data for **5** in Figure 6 was obtained with the following refined parameters (energies in cm^{-1}): $J = +0.99$, $D(Fe_{1,3}) = 0$ (fixed), $D(Fe_2) = -11.5$, $g_\perp(Fe_{1,3}) = 2.14$, $g_\parallel(Fe_{1,3}) = 2.01$, $g_\perp(Fe_2) = 2.78$, $g_\parallel(Fe_2) = 2.13$. The positive J value between the terminal and middle iron atoms in this case reveals an antiferromagnetically coupled complex.

The inset of Figure 6 shows the best fit of the magnetization data for **5**, obtained with $D_{1,3}$ fixed to zero. The J value refined to $+0.72$ cm^{-1}, in good agreement with that from the susceptibility fit. Fixing all g values to 2.00 and allowing $D(Fe_{1,3})$ to vary gave a worse fit, but similar values of $J = +1.45$ cm^{-1} and $D(Fe_{1,3}) = 0.09$ cm^{-1} resulted, as can be seen in Figure S4. The above fits suggest that the $J = +1$ cm^{-1} and $D(Fe_{1,3}) = 0$ cm^{-1} values are well determined.

$[Fe_3(O_2CPh)_6(PheMe_3Eda)_2]$ (6). Modeling of the magnetic data for this compound gave results similar to those for **5**, the other antiferromagnetically coupled compound. Fixing $D(Fe_{1,3}) = 0$ yielded $D(Fe_2) = -11.3$ cm^{-1}, with $J = +1.0$ cm^{-1}, and the fit of the susceptibility data corresponding to these parameters is shown in Figure S5. Although some of the g values fluctuated far from $g = 2.00$, the J value is positive as expected for antiferromagnetic coupling and similar in magnitude to that of **5**.

As found for the ^{i}PrOx complex, a good fit of the magnetization data for **6** resulted in a J value near $+1$ cm^{-1} and a $D(Fe_{1,3})$ value close to zero, as shown in the inset of Figure S5. When the g values were fixed to 2.00, the fit was of lower quality, as seen in Figure S6, but the J and D values remained close to those obtained by the other susceptibility and magnetization fits.

General Comparisons. The large deviations from 2.00 for some of the refined g parameters for **5** and **6** are probably due to other interactions not taken into account by our model, as discussed above for the g values of the BIPhOH compound. The consistency of the J and D values for both **5** and **6** is noteworthy, given the expected similarity in magnetic behavior for these two antiferromagnetically coupled, structurally similar compounds. The Kambé-type model was more successful in fitting the magnetization data for **5** and **6** than for the ferromagnetic compounds. The success of the Kambé-type fit, which does not include any terms for zero-field splitting for these cases, may be correlated with the D values near zero determined for the terminal iron atoms. The negligible D value for $Fe_{1,3}$ obtained from the theoretical analysis is in satisfying agreement with the most important structural difference, the Fe_t-O_d distance, between complexes **5** and **6** as a class and the other three ferromagnetically coupled compounds. As discussed above, the shorter Fe_t-O_d distances in **5** and **6** give the terminal ferrous sites a geometry much closer to octahedral symmetry than the corresponding sites in **1**, **3**, and **4**. Accordingly, one might expect the zfs for these terminal iron atoms to be much smaller than in the less symmetric terminal sites of **1**, **3**, and **4**.

As described above, the reduced magnetization for the ferromagnetically coupled complexes approaches the theoretical value for an $S = 6$ system at high field, but the antiferromagnetically-coupled systems exhibit curves in which $M/N\mu_B$ largely exceeds the value expected for an $S = 2$ ground state. In order to explain this behavior, we describe the magnetics of the system in terms of the instructive approach employed by Kahn and coworkers in reporting high-field magnetization data for the structurally similar complex $[Mn_3(OAc)_6(bpy)_2]$.[64] The authors neglected zero-field splitting and, as appropriate for a d^5 high-spin system, used an isotropic $g = 2.0$ in their theoretical model. This treatment is equivalent to the Kambé model and relies on the Heisenberg Hamiltonian shown in eq 2, from which the relative energies of the spin states can be calculated by using the expression for the eigenvalues (eq 3), where $J = J_{12} = J_{23}$, $S_{13} = S_1 + S_3$, and $S_T = S_{13} + S_2$.

$$\mathcal{H} = J(S_1 \cdot S_2 + S_2 \cdot S_3) + J_{13} S_1 \cdot S_3 \quad (2)$$

$$E(S_T, S_{13}) = J/2[S_T(S_T + 1)] - J/2[S_{13}(S_{13} + 1)] + J_{13}/2[S_{13}(S_{13} + 1)] \quad (3)$$

Use of eq 3 with the addition of a Zeeman term, $\mathcal{H}_{Zeeman} = g\beta B_z M_s$, leads to the simplified diagram for our antiferromag-

(63) Tinkham, M. *Proc. R. Soc. London* **1958**, *A245*, 156−174.

(64) Ménage, S.; Vitols, S. E.; Bergerat, P.; Codjovi, E.; Kahn, O.; Girerd, J.-J.; Guillot, M.; Solans, X.; Calvet, T. *Inorg. Chem.* **1991**, *30*, 2666−2671.

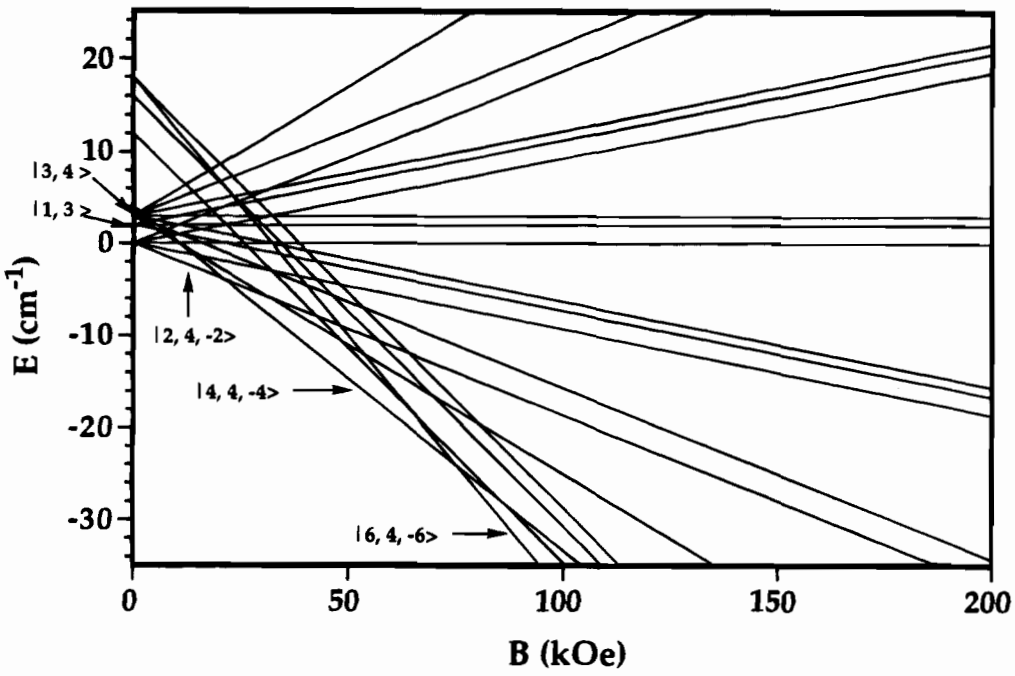

Figure 7. Schematic energy level diagram of complexes **5** and **6** showing the relative energies of the lower spin state manifolds vs applied magnetic field.

netically coupled complexes depicted in Figure 7, in which the energies of selected spin state manifolds are plotted against magnetic field. This plot was constructed with $g = 2.0$, J_{13} set to zero, and $J = +1$ cm^{-1}, values close to those obtained from the above fits (Table 12). As can be seen in Figure 7, the small J value brings the low-lying excited states $|S_T,S_{13}\rangle = |1,3\rangle$ and $|3,4\rangle$ within 5 cm^{-1} of the $|2,4\rangle$ ground state in zero field, and the Zeeman interaction causes the $|S_T,S_{13},M_s\rangle = |4,4,-4\rangle$ state to cross the ground state $|2,4,-2\rangle$ at a field close to 20 kOe. With such a small J value, antiferromagnetic exchange coupling cannot compete with the applied field and, just below 100 kOe, the fully *ferromagnetic* state $|S_T,S_{13},M_s\rangle = |6,4,-6\rangle$ becomes the new ground state. These spin-state crossovers at high field result in the new ground states becoming selectively populated and readily account for the increase in $M/N\mu_B$ above the value predicted for an antiferromagnetic, $S_T = 2$ ground state.

This picture is an extreme simplification of the true energy level diagram for our compounds, even when one only considers $B = B_z$, since zfs effects have been neglected. Zero-field splitting removes the degeneracy of the single-ion spin states so that the spin-coupled levels cannot be represented by the "pure" states shown in Figure 7. In particular, inclusion of rhombic zfs ($E \neq 0$) terms would extensively mix the states. This state mixing caused by the significant zero-field splitting of each Fe(II) ion is probably the cause of the absence of sharp "steps" in the high-field magnetization data for **5** and **6**, in contrast to the trimanganese(II) system.[64] Nevertheless, the qualitative picture represented by Figure 7 remains valid for compounds **1** and **3**−**6**, in which the Zeeman effect can cause state crossover(s) at sufficiently high field.

EPR Studies. Given the recent interest in integer-spin EPR signals for the diiron(II) reduced forms of MMOH,[7-9,11] R2,[12] and deoxyHrN$_3$,[6,10,11] we wondered whether a similar feature might arise in our trinuclear ferrous systems, which also have integer-spin ground states. The X-band (9.43 GHz) EPR spectra for compounds **1**, **3**, and **4** ($S_{total} = 6$ ground state) at 4 K are displayed in Figure 8. These spectra were recorded on solid crystalline samples, diminishing the possibility of a signal arising from lower nuclearity ferrous species that may be present in solution if the trinuclear unit were to dissociate. All three

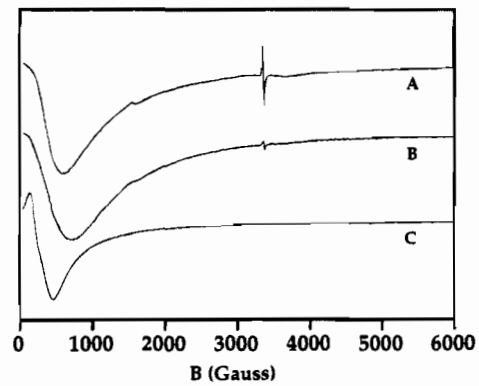

Figure 8. X-band EPR spectra at 4 K for polycrystalline samples of complexes (A) **1**, (B) **3**, and (C) **4**. The sharp $g \approx 2.0$ signal is an impurity in the parafilm used for sample preparation.

complexes show a broad feature at very low field, and for compounds **1** and **4** the trough of the signal is centered at ≈500 G, while for **3** the trough is closer to 700 G. These spectra at least qualitatively bear a strong resemblance to those observed for the diiron(II) forms of the proteins and model complexes discussed above.

Extraction of specific magnetic parameters from these EPR spectra was not possible, but use of the analytical procedures described in the Experimental Section allowed for investigation into their origin. Parameters derived from the magnetic measurements were used to determine possible EPR transitions. For example, use of $J = -5.0$ cm^{-1}, $D(Fe_{1,3}) = 6.0$ cm^{-1}, and $D(Fe_2) = 5.0$, and all g values $= 2.00$[65] resulted in EPR-allowed transitions (with $B_1 \perp B_0$; the transitions are with $B_0 = B_x$, that is, perpendicular to the zfs axis) from the ground (state 1) to the first excited (state 2) state. This transition is highly field-dependent; it occurs at $g_{obs} = \Delta E/\beta B = 90$ for $B = 400$ G but at $g_{obs} = 60$ for $B = 600$ G. These calculated EPR-allowed transitions, from states thermally populated at ≈4 K, have ΔE

(65) The single ion g values determined from the magnetic fits deviate from 2.00, but this effect is minor relative to zero field splitting contributions at these low magnetic fields. For example, increasing g by 10% from 2.0 to 2.2 changes g_{obs} by <1%.

≈ 1 cm^{-1}, which is far from resonance with the microwave quantum (0.314 cm^{-1} at 9.43 GHz).

Rhombic zfs terms ($E_i \neq 0$) were not included in the magnetic fits, where their contributions are relatively less important, but their effect on EPR transitions, particularly in integer-spin systems, is quite significant.[10,58,62] For example, the above calculation with inclusion of the very small term $E(Fe_{1,3}) = 0.06$ cm^{-1} (i.e., $|E/D| = 0.01$), leads to $1 \rightarrow 2$ transitions at $g_{obs} = 82$ and 56 and $2 \rightarrow 3$ transitions at $g_{obs} = 21$ and 14.5 at $B = 400$ G and 600 G, respectively. The actual situation is far more complex in that, as found for mono- and dinuclear integer-spin systems,[58,62] there is probably a distribution of E values. In an individual molecule, each of the three ferrous sites could have slightly differing E values. These subtle differences can significantly affect the EPR transitions. The above parameters, but with $E(Fe_3) = 0.03$ cm^{-1}, yield the $2 \rightarrow 3$ transition in exact resonance with the microwave quantum $\Delta E \approx 0.3$ cm^{-1}, at $g_{obs} = 15.9$ and 11.2 at $B = 400$ and 600 G, respectively. From these considerations, it is apparent that, as the magnetic field is swept, a variety of EPR transitions from different molecules come into partial resonance, giving rise to the observed broad envelope at low field.

Conclusions

We have synthesized and crystallographically characterized four new linear, trinuclear ferrous complexes using either of two general and convenient synthetic routes. This series of carboxylate-bridged triiron(II) complexes has allowed us to correlate well-defined structural differences with a shift from ferromagnetic to antiferromagnetic coupling. Both susceptibility and high-field magnetization data were collected for all compounds and fit to a model allowing for zero-field splitting and **g** anisotropy, yielding reliable exchange-coupling constants (J), axial zfs parameters (D), and axial g values for all complexes. In the case of the high-field magnetization experiment, the Kambé model failed to give a good fit of the data, demonstrating the distinct advantages and necessity of the more sophisticated theory used here.

Integer-spin, low-field EPR spectra were observed for the ferromagnetically coupled complexes. These signals are quite similar to those observed for the diiron(II) forms of the proteins MMOH, deoxyHrN_3, and R2 and models of their diiron(II) cores, demonstrating that such signals taken alone cannot distinguish between a dinuclear and trinuclear ferrous core. Simple calculations showed that such EPR-allowed signals are expected for these trinuclear systems with $J \leq D \leq 10$ cm^{-1}.

Finally, weak exchange coupling, $|J| \leq 5$ cm^{-1}, occurs between adjacent ferrous ions with mono- and bidentate carboxylate bridges, the sign of J depending upon small perturbations in the geometry at each ferrous site. In particular, it appears that a geometry closer to idealized octahedral symmetry, which would minimize $|D|$, at the terminal ferrous sites favors antiferromagnetic exchange; significant axial distortion, which would maximize $|D|$, at these sites favors ferromagnetic exchange. There may be a relation between this observation for linear trinuclear iron(II) complexes and the finding that, in linear triiron(III)[66,67] and trimanganese(II)[64] complexes which contain single ions having $^6A_1$ ground states, there is antiferromagnetic coupling.

Acknowledgment. This work was supported by a grant from the National Institute for General Medical Sciences. We thank E. McNiff, Jr., of the Francis Bitter National Magnet Laboratory for obtaining the high-field magnetization data, K. E. Liu for assistance in obtaining the EPR spectra, and Professor L. Que, Jr., for helpful discussions.

Supplementary Material Available: Tables of complete crystallographic data, bond distances, bond angles, and atomic positional and thermal parameters for **3**–**6**, ORTEP diagrams for **3** and **6**, and plots of the susceptibility and high-field magnetization data for **3**, **4**, and **6** (57 pages). Ordering information is given on any current masthead page.

IC941336A

(66) Vankai, V. A.; Newton, M. G.; Kurtz, D. M., Jr. *Inorg. Chem.* **1992**, *31*, 343–345.

(67) Kitajima, N.; Amagai, A.; Tamura, N.; Ito, M.; Moro-oka, Y.; Heerwegh, K.; Pénicaud, A.; Mathur, R.; Reed, C. A. *Inorg. Chem.* **1993**, *32*, 3583–3584.